Design, Fabrication, and CMOS Integration of MEMS Humidity Sensors

Tanmoy Saha
Wireless ICs and MEMS Laboratory
Department of Electrical and Computer Engineering
McGill University, Montreal, Canada
July 2012

A thesis submitted to McGill University in partial fulfillment of the requirements of the degree of master of Engineering.
© Tanmoy Saha, 2012.

Abstract

The design, microfabrication, and CMOS integration of micro-electro-mechanical systems (MEMS) capacitive humidity sensors are presented in this work. Theoretical analysis and simulations were done to understand how sensor performance can be optimized. While CoventorWare was used for steady-state simulations, a MATLAB simulation model, based on the mathematics of moisture adsorption and diffusion, was developed for dynamic simulations. The sensors were fabricated using a process flow that has a low thermal budget ($\leq 300\ ^{\circ}C$), as well as material and chemical compatibility with IC fabrication, allowing it to support monolithic integration with CMOS circuitry for system-on-chip (SoC) designs. The fabricated sensors were tested using both deliquescent calibration salts and a humidity / temperature chamber, providing results that were used to compare the performance of various sensor designs. These experimental results, along with the simulation results, were used to devise and justify a design methodology for MEMS capacitive relative humidity sensors. The sensors showed high sensitivity over a large dynamic range, response times as fast as 1.5 seconds, and excellent long term drift as low as 0.1 %RH/year.

The humidity sensors were fabricated on top of CMOS dies (TIA - transimpedance amplifier) obtained from Texas Instruments to demonstrate the capability of full monolithic integration of the MEMS sensors and IC. A very convenient and versatile methodology was reported and used for integrating the MEMS sensors above IC dies of any size. Test results show that the performance of the TIA is unaffected by the integration, while the MEMS sensors grown on top of the TIA are fully functional, thereby validating the integration procedure used and the IC-compatibility of the MEMS humidity sensor process flow.

Sommaire

La conception, le microfabrication, et l'intégration de CMOS des sondes capacitives micro-électro-mécaniques d'humidité des systèmes (MEMS) sont présentés dans ce travail. L'analyse et les simulations théoriques ont été faites pour comprendre comment l'exécution de sonde peut être optimisée. Tandis que CoventorWare était employé pour des simulations équilibrées, un modèle de simulation de MATLAB, basé sur les mathématiques de l'adsorption et de la diffusion d'humidité, a été développé pour des simulations dynamiques. Les sondes ont été fabriquées en utilisant un écoulement de processus qui a un bas budget thermique (○C de ≤ 300), comme la compatibilité de matériel et de produit chimique avec la fabrication d'IC, lui permettant de soutenir l'intégration monolithique avec des circuits de CMOS pour des conceptions du système-sur-puce (SoC). Les sondes fabriquées ont été examinées en utilisant les deux sels déliquescents de calibrage et une chambre d'humidité/température, fournissant les résultats qui ont été employés pour comparer l'exécution de la diverse sonde conçoit. Ces résultats expérimentaux, avec les résultats de simulation, ont été employés pour concevoir et justifier une méthodologie de conception pour les sondes capacitives d'humidité relative de MEMS. Les sondes montrées la sensibilité élevée au-dessus d'une gamme dynamique étendue, des temps de réponse plus rapidement que 1.5 seconde, et d'une excellente dérive à long terme aussi basse que 0.1 % RH/year.

Les sondes d'humidité ont été fabriquées sur les matrices de CMOS (TIA - amplificateur de transimpedance) obtenues à partir de Texas Instruments pour démontrer les possibilités de la pleine intégration monolithique des sondes et de l'IC de MEMS. Une méthodologie très commode et souple a été rapportée et employée pour intégrer les sondes de MEMS au-dessus des matrices d'IC de n'importe quelle taille. Les résultats d'essai prouvent que l'exécution du TIA est inchangée par l'intégration, alors que les sondes de MEMS développées sur le TIA sont entièrement fonctionnelles, validant de ce fait le procédé d'intégration utilisé et l'IC-compatibilité de l'écoulement de processus de sonde d'humidité de MEMS.

Acknowledgements

I would like to thank my supervisor, Professor Mourad N. El-Gamal, for giving me the opportunity to work with him on this interesting project and for his unrelenting support. I was the first student in the McGill Wireless ICs and MEMS Lab to demonstrate functional MEMS sensors and I really appreciate having got this opportunity.

I would also like to deeply thank Mr. Karim Allidina, Mr. Paul Vahe-Cicek, Ms. Sareh Madahvi, Ms. Qing Zhang, and Professor Frederic Nabki for helping and supporting me all throughout this project. They have always provided me with valuable advice and helped me with design reviews, microfabrication processes and techniques, and test setups. I am really very grateful to them.

I also greatly appreciate the help and support I received from the staff of the McGill microfabrication facility, namely Mr. Matthieu V. Nannini, Mr. Donald W. Berry, and Mr. John Li. In addition, I would like to thank Mr. Laurent Mouden, lab manager of the LASEM lab at Polytechnique University, for providing me with packaging and wire-bonding services.

Last, but not least, I would like to thank my parents who have continuously supported me.

Table of Contents

Abstract ---2

Sommaire ---3

Acknowledgements ---4

Table of Contents ---5

List of Figures and Tables ---7

1. Introduction --- 10

1.1. Classification of Humidity Sensors --- 11

—— 1.1.1. Relative Humidity (RH) --- 12

—— 1.1.2. Dew/Frost Point (D/F PT) --- 12

—— 1.1.3. Parts Per Million (PPM) --- 14

1.2. Types of Relative Humidity Sensors --- 14

—— 1.2.1. Thermal Conductivity Relative Humidity Sensors --- 15

—— 1.2.2. Gravimetric Relative Humidity Sensors --- 18

—— 1.2.3. Resistive Relative Humidity Sensors --- 22

—— 1.2.4. Capacitive Relative Humidity Sensors --- 24

1.3. Moisture Sensing Materials --- 26

—— 1.3.1. Metal Oxides / Ceramics --- 26

—— 1.3.2. Porous Silicon --- 28

—— 1.3.3. Porous Silicon Carbide --- 29

—— 1.3.4. Polymers --- 29

—— 1.3.5. Carbon Nanotubes (CNTs) --- 32

1.4. Main Contributions of this Work --- 32

1.5. References --- 34

2. Design/Simulation --- 38

2.1. Sensor Type and Sensing Material --- 38

2.2. Structure and Geometry --- 39

2.3. Simulation --- 42

—— 2.3.1. Steady-State Simulations (CoventorWare) - --- 42

—— 2.3.2. Dynamic Simulations (MATLAB Simulation Model) --- 49

2.4. Process Flow ---------- 52
2.5. Design Parameters ---------- 55
2.6. Additional Process Flow Steps ---------- 56
—— 2.6.1. Heating the Sensor ---------- 56
—— 2.6.2. Reference Device ---------- 58
2.7. MATLAB Simulation Model ---------- 60
—— 2.7.1. Theory of Capacitive Humidity Sensing ---------- 60
—— 2.7.2. Simulation Model ---------- 63
2.8. References ---------- 66
3. Fabrication/Testing / CMOS Integration ---------- 67
3.1. Microfabrication ---------- 67
—— 3.1.1. Packaging ---------- 67
3.2. Testing Procedures and Results ---------- 67
—— 3.2.1. Deliquescent Salts Testing ---------- 67
—— 3.2.2. Sensitivity / Hysteresis Testing ---------- 70
—— 3.2.3. Response Time Testing ---------- 73
—— 3.2.4. Stability Testing ---------- 78
—— 3.2.5. Long Term Drift ---------- 79
—— 3.2.6. Reference Device Testing ---------- 81
3.3. CMOS Integration ---------- 82
—— 3.3.1. Background on MEMS/CMOS Integration ---------- 82
—— 3.3.2. CMOS Integration Process Description ---------- 85
—— 3.3.3. CMOS Integration Test Results ---------- 90
3.4. References ---------- 94
4. Conclusion ---------- 96
4.1. Design Strategy ---------- 96
4.2. Future Work ---------- 98
4.3. Summary ---------- 99

List of Figures and Tables

FIGURES

Figure 1-1: Correlation between the three units of humidity measurement----------------- 11
Figure 2-1: Example of thermal conductivity RH sensor-------------------------------------- 16
Figure 3-1: Thermal conductivity RH sensor using -- 17
Figure 4-1: Surface Acoustic Wave humidity sensor --- 20
Figure 5-1: Cantilever Resonator --- 21
Figure 6-1: Clamped-clamped beam resonator -- 22
Figure 7-1: (a) Cantilever based resistive humidity sensor and (b) the layout of the platinum layer --- 23
Figure 8-1: Electrode based resistive humidity sensor--- 24
Figure 9-1: Cantilever based capacitive humidity sensor ------------------------------------- 25
Figure 10-1: Lateral (left) and stacked (right) structures for electrode-based capacitive humidity sensors --- 25

Figure 1-2: Capacitive humidity sensing devices - (a) Design-A: top electrode with square holes and (b) Design-B: top electrode as rectangular fingers --------------------------- 40
Figure 2-2: Cross-section of the capacitive humidity sensor --------------------------------- 40
Figure 3-2: Plot of sensor sensitivity against its top electrode thickness for (a) Design-A and (b) Design-B--- 44
Figure 4-2: Plot of sensor sensitivity against its polymer thickness for (a) Design-A and (b) Design-B--- 45
Figure 5-2: Plot of sensor sensitivity against the top electrode width for (a) Design-A and (b) Design-B--- 46
Figure 6-2: Plot of sensor sensitivity against the top electrode gap for (a) Design-A and (b) Design-B--- 46
Figure 7-2: Plot of sensor sensitivity against the thickness of the patterned bottom electrode for (a) Design-A and (b) Design-B-- 48

Figure 8-2: Cross-section diagram indicating larger air region for fringing fields due to patterned bottom electrode -- 48
Figure 9-2: Normalized capacitance change for Designs-A and B for a 25 %RH step --- 50
Figure 10-2: Response variation as top metal width (W) is increased---------------------- 51
Figure 11-2: Fabrication process flow (horizontal cross-sections shown) ------------------ 53
Figure 12-2: Sensing structure on top of a metal heater -------------------------------------- 56
Figure 13-2: Process steps for including a heater layer below the sensor------------------- 57
Figure 14-2: Sensing device alongside a reference device ------------------------------------ 59
Figure 15-2: Additional process steps for creating reference devices (horizontal cross-sections shown) -- 60
Figure 16-2: Steps involved in capacitive humidity sensing--------------------------------- 61
Figure 17-2: Simulation model-- 64

Figure 1-3: Packaged die with sensors -- 67
Figure 2-3: Deliquescent Salts Testing Setup -- 68
Figure 3-3: Sensor capacitance against relative humidity obtained using deliquescent salts testing-- 70
Figure 4-3: Measured sensor capacitance against relative humidity------------------------- 71
Figure 5-3: Maximum hysteresis of several devices with both flat and patterned bottom electrodes --- 73
Figure 6-3: Response Time Test Setup--- 74
Figure 7-3: Response time plot of to devices along with the simulation result ------------ 75
Figure 8-3: Comparison of responses of sensors with different top electrode patterns --- 77
Figure 9-3: Plot showing the recovery times of fast and slow devices for both Design-A and Design-B type devices --- 78
Figure 10-3: Plot of capacitance against relative humidity for a device with and without 900 nm parylene shield -- 82
Figure 11-3: TIA die obtained from Texas Instruments -------------------------------------- 85
Figure 12-3: Cross-section diagram of die on carrier wafer showing edge-beading effect from spin-coating photoresist -- 86
Figure 13-3: Steps for die mold fabrication and carrier attachment ------------------------ 88

Figure 14-3: CMOS die mold with the CMOS die inside the mold-------------------------- 89
Figure 15-3: TIA CMOS die with MEMS sensor on top -------------------------------------- 91
Figure 16-3: S-parameter plot for bare TIA die and TIA die with sensor grown on top -- 91
Figure 17-3: Sensor capacitance vs. relative humidity for the MEMS sensor grown on top of CMOS die -- 92
Figure 18-3: Sensor capacitance vs. relative humidity for 3 different test runs ------------ 93
Figure 19-3: Relative humidity step (40 %RH to 70 %RH) response of sensor device grown on top of CMOS die along with the response of the stand-alone sensor and the simulation response-- 94

TABLES

Table 1-2: Response time corresponding to the various top metal widths (*W*)------------- 51

Table 1-3: Deliquescent salt/de-ionized water ratio and corresponding relative humidity69
Table 2-3: Measured and simulated response time values for Design-A and Design-B type devices of varying *W* -- 75
Table 3-3: Recovery and response time values of fast and slow devices for both Design-A and Design-B type -- 78
Table 4-3: Performance parameters for the MEMS sensor on top of CMOS die ---------- 92

Table 1-4: Various sensor sizes that can be fabricated-- 98

1. Introduction

Humidity is the amount of water vapor in the air. Its measurement is referred to as *Hygrometry*. Water vapor is a natural component of air and its measurement is very important in a wide variety of applications, including:

- Medicine / health care - respiratory equipment, sterilizers, incubators, pharmaceutical processing, and biological products.
- Domestic – living environment control in buildings (human comfort), cooking appliances, laundry, etc.
- Agriculture – green-house air-conditioning, plantation protection, soil moisture monitoring, storage, etc.
- Semiconductor industry – wafer processing, clean room environment control for the technical requirements of machines and processes, etc.
- Automobile industry – rear window defoggers, motor assembly lines, etc.
- Food production / processing and storage
- Climatology / Meteorology
- General industry – dryers, ovens, film desiccation, paper and textile production, etc.
- Heating, ventilating, and air-conditioning (HVAC) systems – indoor environment control such as houses, industrial and office buildings, museums, automobiles, and planes as well as marine environment control such as aquariums.

This wide variety of applications makes humidity one of the most frequently measured physical quantities. Devices used to measure water vapor content in the atmosphere are known as humidity sensors. Temperature is another quantity that is measured as much as humidity. While, temperature measurement today can be done quite easily and with very high accuracy, hygrometry is much more complex. There exists a whole multitude of techniques for humidity measurement and no one method can meet all requirements of

every application. Every application has different specifications and operating conditions. Due to this, there exists a wide variety of humidity sensors and sensing materials.

There has always been a growing interest to miniaturize sensors in order to develop compact, low power, low cost, reliable and high performance sensor Microsystems. Micro-electro-mechanical systems (MEMS), is a very promising and emerging technology for miniaturizing and batch fabricating sensor devices in order to reduce the size and cost of devices. MEMS fabrication allow for a high level of redundancy – multiple devices can be fabricated together to form one very reliable system which serves to reduce the effect of defect or variations as well as increase functionality and performance. MEMS technology allows for CMOS-compatible fabrication process in which sensors can be integrated on the same substrate as the interface circuitry, thereby enabling the entire system to be on one chip.

1.1. Classification of Humidity Sensors

The measurement of the amount of water vapor in a gas, such as air, is referred to as humidity measurement and the most commonly used measurement units are:

- Relative Humidity (RH)
- Dew / Frost Point (D/F PT)
- Parts Per Million (PPM)

Fig. 1-1 shows the correlation between the three measurement units.

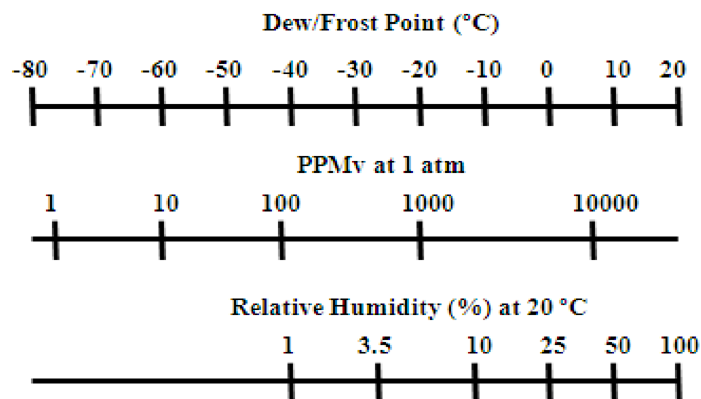

Figure 1-1: Correlation between the three units of humidity measurement [33]

1.1.1. Relative Humidity (RH)

As can be seen from Fig. 1-1, relative humidity (RH) covers the higher humidity range. RH can be defined as the ratio of the mass of water vapor in a unit volume of air (or a gas) to the mass of water vapor which that volume could hold if the vapor were saturated at a specific temperature. It is the ratio of the partial pressure of water vapor in air (or a gas) to the saturation vapor pressure of air (or the gas) at a given temperature. The saturation vapor pressure defines the maximum amount of humidity that the air can hold. Beyond this limit, condensation occurs to form fog or water droplets. The RH indicates how far away from this limit the moisture level is by expressing the actual humidity amount as a percentage of the maximum/saturation humidity amount. This can be expressed mathematically as shown in Equation (1), where p_w is the partial vapor pressure, which denotes the actual amount of humidity, and p_s is the saturation vapor pressure.

$$RH = \frac{p_w}{p_s} \times 100\% \quad \dots\dots\dots (1)$$

RH is a function of temperature and it is therefore a relative measurement that is expressed as a percentage. The temperature dependence of relative humidity is due to the saturation vapor pressure being a function of temperature. The maximum amount of water vapor that air can hold is proportional to temperature, whereas the partial vapor pressure is independent on temperature, thereby making relative humidity inversely proportional to temperature. Due to this very reason, it is crucial to know the exact temperature when comparing relative humidity values. On the other hand, the partial water vapor pressure is proportional to the total air pressure according to Dalton's law, but the saturation vapor pressure is independent of total air pressure, making RH to be directly proportional to the total air pressure.

1.1.2. Dew/Frost Point (D/F PT)

Dew point is the temperature at which the water vapor in air (or a gas) condenses to liquid. Frost point is the temperature at which the water vapor in air (or a gas) condenses to ice. Dew point is above 0 $^{\circ}$C and frost point is below 0 $^{\circ}$C. Both are dependent on the

air (or gas) pressure, but not on temperature. As can be seen from Fig. 1, dew / frost point covers all humidity range. Dew point is a more common unit than frost point and the very basic way of measuring it is to cool a surface whose temperature is being measured until water droplets form. Once this happens, the temperature is recorded and that is the dew point.

The dew point is a different unit of moisture level measurement, but has a strong relation to relative humidity. The difference between the dew point and actual ambient temperature is inversely proportional to the relative humidity. In other words, a high relative humidity indicates that the dew point is close to the actual temperature and a low relative humidity indicates that the dew point is further away from the actual temperature. At 100%RH, the dew point is equal to the current temperature.

If pressure remains constant, the dew point at a given temperature is associated with the absolute humidity. Absolute humidity is the mass of water vapor per unit volume of air. If the temperature changes under constant pressure conditions, the dew point remains the same, but the relative humidity changes. Two different systems with different temperatures can have the same relative humidity simply because the system with the higher temperature has a higher dew point (i.e. contains more water vapor per unit volume of air) than the colder system.

If temperature remains constant, the dew point at a given pressure is associated with the specific humidity. Specific humidity is the ratio of water vapor mass to that of dry air. If the pressure changes under constant temperature conditions, the dew point will change in direct proportion to the pressure and so will the relative humidity. A pressure rise increases the relative humidity, bringing the saturation temperature (dew point) closer to the current temperature. Hence, a pressure increase causes a dew point increase and vice versa. If two different systems with different pressures, but the same temperature, have the same dew point, it simply means that both systems have the same absolute humidity, but the lower pressure system has a higher specific humidity.

There are several methods of measuring the dew point, some of which include using photoelectric, resistive, and nucleonic detectors. This work does not focus on dew / frost point measurements and hence, it will not be discussed further. More information can be found in [1].

1.1.3. Parts Per Million (PPM)

Parts per million is also an absolute measurement like dew / frost point. It expresses water vapor content as a volume fraction (mixing ratio). This measurement is difficult to understand and work with, but it is useful when dealing with very small amounts of moisture. It covers low humidity range as can be seen from Fig. 1. This measurement is not very common and is only used in specific industry applications requiring trace moisture measurements.

RH is the most commonly used unit for the measurement of water vapor content. It expresses the vapor content at a specific temperature as a percentage of the concentration required to cause saturation at that temperature. It is very easy to interpret, understand, and process. Absolute humidity measurements (dew / frost point and parts per million) are pressure dependent and difficult to conceive. They are not preferred for most engineering applications. Most applications (including the ones listed in Chapter 1) use relative humidity as the unit for moisture measurement in air or in a gas. As a result, the focus of this work was on relative humidity sensors.

1.2. Types of Relative Humidity Sensors

Relative humidity sensors are used in a wide variety of applications and the specifications they must usually meet include:

- Dynamic Range – this is the range of humidity that can be measured (e.g. 0 %RH to 100 %RH for a full dynamic range).

- Sensitivity – change in the output unit for the sensor for a given change in relative humidity (e.g. if the output is a voltage, V_{out}, that changes with humidity, then the sensitivity is defined as $\Delta V_{out} / \Delta RH$).
- Response time – this is the time it takes for the sensor output to reach 80% or 90% of its final or steady state value for a sudden change in relative humidity.
- Hysteresis – this is the difference in the response paths associated with increasing and decreasing humidity. It is usually recorded as the maximum percentage difference between the 'humidity increase' and 'humidity decrease' response over the entire dynamic range, and the relative humidity level at which this occurs is sometimes specified (e.g. ±5 % hysteresis at 50 %RH).
- Reproducibility / Precision – this measures how much the sensor output varies for the same measurement repeated multiple times under the same conditions.
- Chemical and Physical Stability – the resistance of the sensor and its output to chemicals, other vapors, and physical forces.
- Long-Term Stability – the variation in performance over time.
- Accuracy – The degree of closeness between the measured relative humidity level and the actual level.
- Cost
- Life Span – how long before the sensor cannot be reused anymore.

These specifications are different for different applications and there are various types of relative humidity sensors for achieving these specifications. Some are better for certain specifications than others. The various types of relative humidity sensors are discussed next.

1.2.1. Thermal Conductivity Relative Humidity Sensors

At elevated temperatures (≥ 250 °C), there is a difference in thermal conductivity between dry and humid air. This feature is exploited in thermal conductivity relative humidity sensors. The thermal conductivity of air changes with the humidity level and this can be

measured to determine the relative humidity level. A heat sensitive element is needed to detect the difference in conductivities. Two types are common:

(1) Platinum Metal Resistor

The resistance of platinum films changes with temperature. They have a very high positive temperature coefficient of resistance, high temperature-resistance linearity, and high chemical durability. An example device is shown in Fig. 2-1. This device uses two platinum resistors located on top of two different diaphragms. Other metal resistors can also be used. One is exposed to the atmosphere, while the other is enclosed and filled with nitrogen gas. The exposed element is the sensing element (SE) since it is in contact with the humid air, while the other is a compensating element (CE).

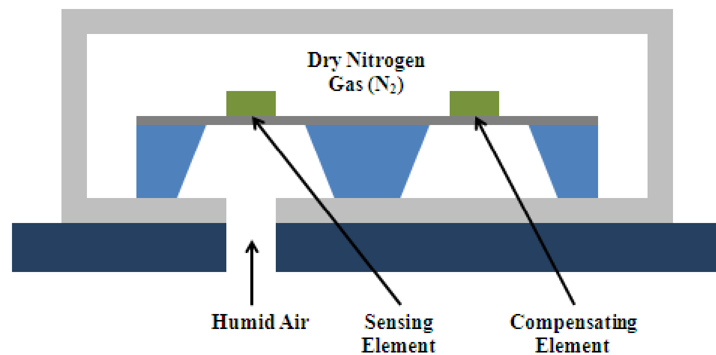

Figure 2-1: Example of thermal conductivity RH sensor [2]

Both resistors are heated up electrically to temperatures of around 250 °C so that there is a measurable difference in thermal conductivity between dry and humid air. In such a scenario, an increase in humidity causes the conductivity of the humid air around the sensing element to increase. This causes a decrease in the temperature of the sensing element and a corresponding decrease in the resistance of the platinum resistor. Since the compensating element is not exposed to humid air, its resistance stays the same. However, the resistance change due to ambient temperature is the same for both elements and that cancels out.

The resistance outputs of both elements are processed using integrated electronics to produce a final voltage output which changes with relative humidity. Sensitivities of around 0.6 mV/%RH, response times as low as 5 s, recovery times as low as 25 s, and

< 2% hysteresis have been reported for such devices [2]. These devices have a lower detection limit of around 40 %RH. This is mainly because the difference in thermal conductivities at humidity levels below 40% is very small and hard to measure.

(2) Diodes

Suspended diodes can be used as the sensing elements. Diodes have negative temperature sensitivity – their output voltage decreases with increasing temperature. They usually have higher temperature sensitivities than metal resistors. An example device using diodes as the sensing element is shown in Fig. 3-1.

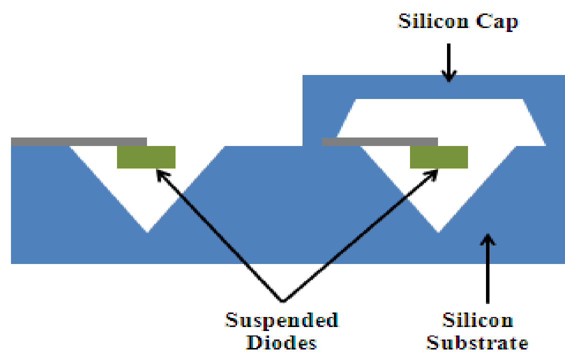

Figure 3-1: Thermal conductivity RH sensor using [3]

The idea is the same as in the metal resistor case. Both diodes are suspended (for substrate isolation) and one is exposed to the atmosphere while the other is enclosed. Both diodes are heated up electrically to about 250 °C (**diodes take less power to be heated up than the metal resistors**). Changes in humidity will cause the thermal conductivity of humid air to change and as a result, the temperature of the left diode (sensing diode) changes while that of the right diode (reference diode) remains the same. The diodes will therefore have different turn-on voltages. The turn-on voltage of the sensing diode will change with humidity and that of the reference is independent of humidity. Integrated circuits are used to convert the difference between the diode voltages to produce an overall output signal which changes with relative humidity. The sensor and the electronics can be integrated on the same chip.

Sensitivities as high as 47 mV/%RH, <1% hysteresis, 20 to 90 %RH dynamic range, and around 1.38 mW power consumption have been reported for such devices [3]. Another

advantage of using diodes instead of metal resistors is that the lower detection point (20 %RH in this case) is lower than metal resistor devices (~40 %RH).This is probably due to the higher temperature sensitivities of diodes causing them to be able to detect the small thermal conductivity differences at low humidity levels.

Most of the thermal conductivity relative humidity sensors are similar in concept to the above two. They usually exhibit high linearity, long-term stability and long-life, and good chemical durability. They can be used in harsh environments. Response times as low as 40 ms have been reported [4]. They are operated at elevated temperatures – hence, there is no water condensation at high humidity and dust/other particles are kept off, but constant heating is required, making them very power hungry. Their sensitivities increase with heating temperature, but that calls for more power consumption and higher temperatures can melt the metal resistors and/or other layers in the device. The fact that cavities have to be created in the substrate and the compensating element has to be hermetically sealed from the environment makes the fabrication process complicated.

1.2.2. Gravimetric Relative Humidity Sensors

Gravimetric relative humidity sensors detect mass changes due to adsorption/absorption of moisture causing changes in resonant frequency. A resonant device is coated with a moisture sensitive material. This material adsorbs/absorbs the moisture causing a change in mass and a resulting shift in the resonant frequency. There are various types of gravimetric humidity sensors depending on the type of resonant device:

(1) Quartz Crystal Microbalance (QCM)

This uses a quartz crystal resonator to detect mass changes which translates to humidity changes. A quartz crystal resonator uses the mechanical resonance of piezoelectric quartz crystals to produce very precise electrical resonant frequencies. It consists of a piezoelectric quartz crystal with two metal electrodes on opposite sides. The resonant frequency is disturbed if the mass on the surface of the resonator (metal plates) changes. This property is used to detect humidity changes. QCMs are very sensitive to mass

changes. They can detect very small mass changes and hence, are suited for low humidity levels.

Moisture molecules absorbed on the resonator surface causes a change in the mass of the system and hence a resonant frequency change. If the electrodes are coated with a humidity sensitive (hygroscopic) material, the moisture sensitivity and selectivity can be highly improved. This material sorbs moisture and this causes the mass on the plates to change, causing a shift in the resonant frequency. The amount of moisture sorbed changes with humidity and hence, the resonant frequency of the crystal resonator varies with humidity.

$$\Delta f \propto f_o^2 \Delta m \quad \dots\dots\dots(2)$$

Equation (2) shows that the frequency shift is proportional to the square of the resonant frequency (f_o) and the change in mass (Δm).

The performance of these types of sensors depends on the properties of the coating material. The materials usually used are metals, metal oxides, polymers, carbon nanotubes, and some others. Frequency shifts as high as 4 kHz have been reported using carbon nanotubes for humidity range of about 10 to 82%RH [5]. Response times as low as 1.5 s (from 44 to 99 %RH) has been reported with fullerene coatings [6]. QCMs are very non-linear since the relationship between the resonant frequency and mass is non-linear. Quartz crystals are off-chip components and hence cannot be integrated with the interface circuits. Systems will be fairly large and bulky. They are very sensitive to surface perturbations and require expensive driving and detecting electronics.

(2) Surface Acoustic Wave (SAW) Devices

A surface acoustic wave (SAW) device is shown in Fig. 4-1. In such devices, two sets of interdigitated transducers (IDT) are located on top of a piezoelectric / acoustic substrate. A voltage applied to the input IDT induces strain on the acoustic layer via the reverse piezoelectric effect. This creates a series of acoustic waves which travels along the acoustic layer with a phase velocity (v_0) to the output IDT where they are converted back

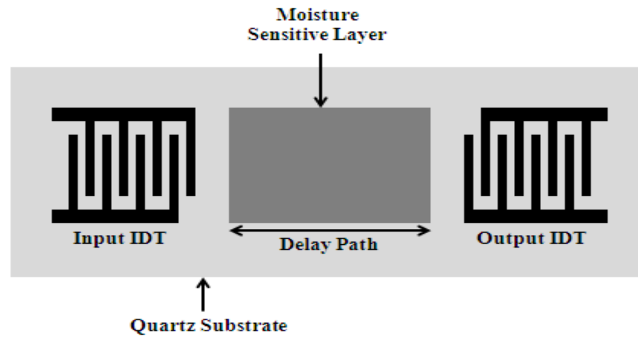

Figure 4-1: Surface Acoustic Wave humidity sensor [1]

to an electrical signal via the piezoelectric effect. When in a closed loop with an amplifier, the device will resonate at a precise frequency. If the travel path is coated with a moisture-sensitive film, moisture is absorbed causing a change in mass, density, permittivity, and electrical conductivity of the film. All these changes induce a change in the surface acoustic wave phase velocity. The change in phase velocity can be measured as a change in the center frequency (f_0) of the device. Hence, the frequency changes with the amount of moisture absorbed or with the amount of humidity in air. The relative changes in phase velocity and frequency is given by:

$$\frac{\Delta v}{v_0} = -\frac{\Delta f}{f_0} \quad \ldots\ldots\ldots(3)$$

Higher harmonics can be used to increase the sensitivity. Some devices use dual delay lines or dual SAW oscillators to cancel out any systematic effects and the sensor only responds to non-systematic changes such as the changes in electrical properties of the sensing film [7].

SAW devices have a much higher mass sensitivity than QCM devices (10 ng/cm^2 compared to 1.2 ng/cm^2), but oscillator instabilities can generally pose problems in practical applications. The sensing material used usually includes metal oxides, ceramics and polymers. The performance of the sensors depends on the choice of the sensing material. Sensitivities of around 80 Hz/%RH [7] have been reported with cellulose acetate sensing layer. Most of the reported SAW sensors are linear for a certain humidity range and then become non-linear. Response times of less than 20 s, good repeatability, high sensitivity, good chemical stability, 0-100 %RH dynamic range, good linearity up to 50

%RH, and low hysteresis have been achieved with Nafion sensing layer [8]. SAW sensors usually have a fair amount of hysteresis and are very sensitive to surface perturbations. SAW systems require expensive detecting and driving electronics.

(3) Cantilever Resonators

A cantilever resonator is shown in Fig. 5-1. A piezoelectric polymer material (polyvinyl-difluorene, PVDF) is used. When an electrical signal is applied to the electrode, the cantilever vibrates as a result of expansion or contraction of the beam. The polymer is moisture-sensitive and sorbs water vapor. This causes a change in mass and hence a change in the frequency. Hence, the frequency changes with the amount of moisture sorbed. The frequencies of these devices are usually low and so are the sensitivities (small frequency shifts over humidity changes). A shift of around 30 Hz was reported for a 0-90 %RH range [9]. Like the other gravimetric sensors, expensive detecting and driving electronics are required.

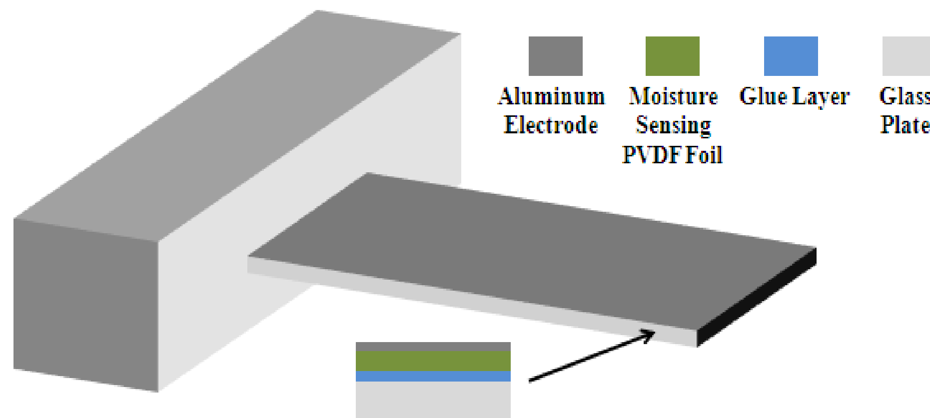

Figure 5-1: Cantilever Resonator [9]

(4) Clamped-Clamped Beam Resonators

Fig. 6-1 shows a clamped-clamped beam resonator. Upon electrical excitation, the beam vibrates at its resonant frequency. This generates a time-varying capacitance and correspondingly outputs a current at the resonant frequency of the beam. If this resonator is put in a closed loop system with an amplifier, an oscillator is obtained which outputs electrical signals at the resonant frequency of the beam.

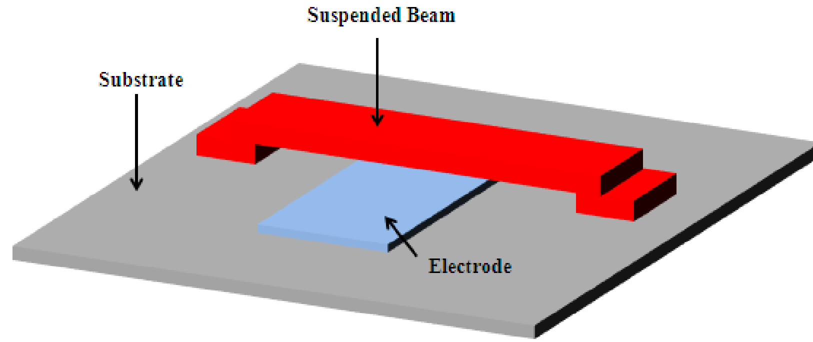

Figure 6-1: Clamped-clamped beam resonator [34]

The output frequency is defined by the following equation:

$$f_o = \frac{\alpha_n^2}{2\pi\sqrt{m}}\sqrt{\frac{EI}{L^3}} \quad \ldots\ldots\ldots(4)$$

In equation (4), *m* is the mass of the beam. If the top of the beam is coated with a hygroscopic layer, moisture will be sorbed into this layer and this will increase the mass of the beam, resulting in a change in the output frequency. The amount of moisture sorbed depends on the surrounding air humidity level and hence, the output frequency of the device will change according to the water vapor content in air.

In the literature review done for this work, this type of humidity sensor was not found reported in any paper. From hand calculations, it can be found that an 8.3 MHz resonator, with a 1 µm polymer sensing layer, can cause a frequency shift of about 10 kHz over 0-100 %RH range (assuming a 2 % mass change over the entire humidity range). Polymers, metal oxides, and carbon nanotubes are potential choices for the sensing layer. Since the frequency-mass relationship is non-linear, the humidity response will be non-linear. Also, these sorts of sensors require expensive driving and detecting electronics. This is true of all gravimetric humidity sensors.

1.2.3. Resistive Relative Humidity Sensors

(1) Cantilever Based

An example of a cantilever based humidity sensor is shown in Fig. 7-1. The polyimide layer is the moisture sensing layer. Polyimide is used as an example; other sensing

materials can be used. A platinum resistor layer is underneath the sensing layer and an example layout of this platinum layer is shown.

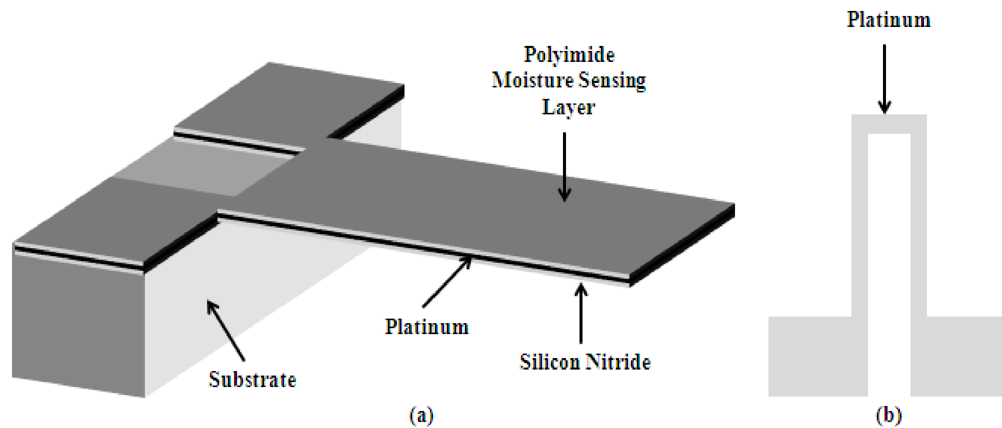

Figure 7-1: (a) Cantilever based resistive humidity sensor and (b) the layout of the platinum layer [10]

The sensing layer (polyimide) sorbs moisture from the surrounding air and this induces stress on the beam. This causes the beam to deflect or deform, resulting in a change in the effective length of the platinum layer. This change can be measured as a change in the resistance of the platinum resistor. The stress induced on the beam, and hence the resistance of the beam, depends on the amount of moisture sorbed by the sensing layer (i.e. depends on the humidity level in the surrounding air).

The sensitivity of these sensors increases with the length of the platinum resistor (length of beam). For a length of 4450 µm, a resistance change of about 150 kΩ was reported over 40-85 %RH with polyimide sensing layer, hysteresis of about 2%, and a response time of about 0.9 s [10]. Cantilever based resistive humidity sensors usually have non-linear behavior and lower detection limits around 30-40 %RH.

(2) Electrode Based

An example of an electrode based resistive humidity sensor is shown in Fig. 8-1 below. There are two sets of interdigitated electrodes (IDEs) arranged as shown in the figure. A moisture sensing layer, whose conductivity changes with humidity, is used to cover both IDEs. When the ambient humidity level changes, so does the conductivity of the sensing layer. This results in a change in the resistance between the two IDEs. Air humidity is

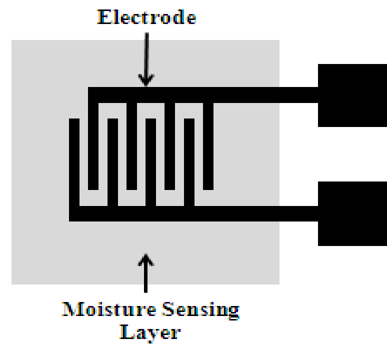

Figure 8-1: Electrode based resistive humidity sensor [1]

transduced into an impedance change. The sensing materials determine their performance and the materials used usually include polymers, electrolytes, ceramics, carbon nanotubes, ceramic/polymer composites, and carbon nanotube/polymer composites. Sensitivity of about 1.6 %/%RH, hysteresis of 0.45%RH, linearity of ±0.05 %RH, and response and recovery times of 17 s and 11 s respectively were reported using MnO-ZnO-Fe_2O_3 film [11].

Electrode based resistive type sensors usually have very high sensitivity. Depending on the sensing layer, rapid response times (~3 s) can be achieved [12]. They tend to have a non-linear response [13], but linearity can be improved with certain sensing layers [12] or composite materials [14]. They usually suffer from significant hysteresis, especially when not used frequently, but low hysteresis can be achieved with some sensing materials [11]. Also, they suffer from the disadvantage that there is an inherent dissipation effect caused by the dissipation of heat due to the current flow in the elements necessary to make measurements. This results in erroneous readings and other problems.

1.2.4. Capacitive Relative Humidity Sensors

(1) Cantilever Based

Cantilever based capacitive humidity sensors work on the same principle as the cantilever based resistive sensors. A cantilever beam is coated with a moisture sensing layer which exerts stress on the beam when moisture is sorbed. The stress causes the beam to bend. Unlike the cantilever resistive sensor, there is no platinum resistor on the beam. Instead, there is metal electrode on top of the beam and another one held a certain distance above

the beam as shown in Fig. 9-1. The glass cover with the second electrode is bonded to the bottom substrate. The bending of the beam changes the distance between the two electrodes, resulting in a capacitance change.

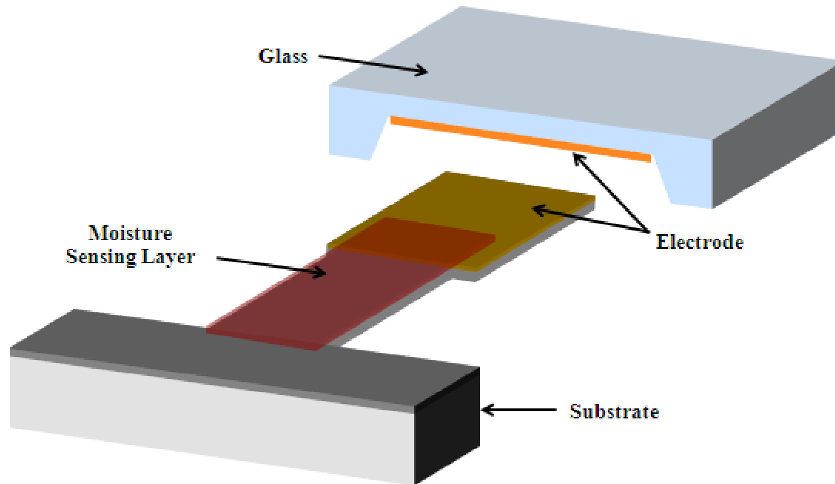

Figure 9-1: Cantilever based capacitive humidity sensor [15]

Sensitivities around 2 nF/%RH (from 45 to 95 %RH), high linearity, response times as low as 1.1 s (from 20 to 40 %RH), and hysteresis of about 1.9% have been reported using polyimide sensing layer [15].

(2) Electrode Based

A moisture sensing layer, whose electrical permittivity changes with the amount of moisture sorbed, is used as the dielectric material between two metal electrodes. Hence, the capacitance between the electrodes changes with the amount of moisture in air. Both lateral [16] and stacked [17] capacitive structures can be used as shown in Fig. 10-1.

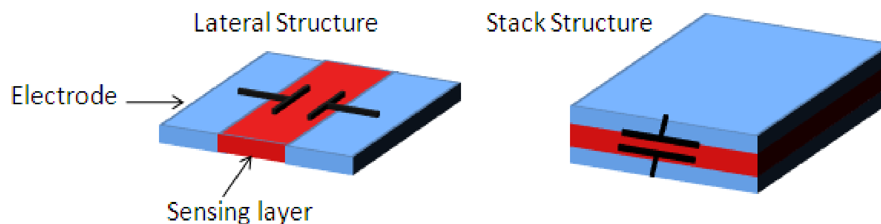

Figure 10-1: Lateral (left) and stacked (right) structures for electrode-based capacitive humidity sensors

The sensing layers define their performance and usually include metal oxides/ceramics, polymers, carbon nanotubes, porous silicon, etc. With barium titanate as the sensing

layer, a non-linear response with 430 % sensitivity, 13 min response time, and 4.5 % hysteresis was obtained [18]. On the other hand, with a polyimide sensing layer, a highly linear response with 20 % sensitivity, 2.5 s response time, and 0.6 % hysteresis was obtained [17].

Electrode based capacitive humidity sensors are the most common humidity sensors. They make up 75% of the market. These sensors offer very high linearity, sensitivity, stability in a wide humidity range, and robustness. They have very low power consumption, no moving parts, and high output signals. Due to slow dehumidification, they usually suffer from hysteresis, but this largely depends on the sensing material. Low hysteresis capacitive humidity sensors have been reported [17].

1.3. Moisture Sensing Materials

There is a wide variety of materials that can be used for humidity sensing. These materials determine the overall response and performance of the humidity sensors. It is very difficult to pin-point one material that can satisfy all requirements. Hence, materials are chosen based on the application and specifications required. The properties usually demanded for humidity sensing materials mainly include high sensitivity over the entire humidity range and temperature, small response and recovery times, high linearity, low hysteresis, high stability to use over time and thermal cycling, high stability to chemicals and other vapors, insolubility in water, and ability to maintain performance in high humidity environments. Some of the most common sensing materials are discussed next.

1.3.1. Metal Oxides / Ceramics

These materials possess a unique structure consisting of grains, grain boundaries, surfaces, and pores. They have high surface-to-volume ratio and abundant void fraction. Their porous nature allows for water vapor to be adsorbed onto their surface. The vapor molecules easily pass through the pores and as humidity increases, they condense in the capillary-like pores between the grain surfaces (phenomena known as capillary

condensation). The adsorption of moisture on their surface changes their electrical properties (conductivity and/or permittivity). Hence, these sensing materials can be used in both resistive and capacitive humidity sensors. The adsorbed vapor molecules also serve to increase the mass of the sensing material – this implies ceramics/ metal oxides can be used in gravimetric humidity sensors as well.

The humidity sensing performance of ceramic / metal oxide sensors are highly dependent on the porosity and surface morphology (size and distribution of pores) of the ceramic or metal oxide sensing layer. Higher porosity or surface area gives higher sensitivity and lower response time. Larger size pores favor reproducibility, stability, and fast response times. Increasing the proportion of smaller-sized pores enhances low humidity performance, while increasing the proportion of large-sized pores enhances high humidity performance. In general, a wide pore-size distribution is preferred to improve performance over all humidity.

Controlling the microstructure and chemical composition of the ceramic or metal oxide material in order to optimize/improve performance or tailor towards a certain set of specifications is a huge part of literature. This is usually done by controlling and/or modifying the preparation steps and conditions, as well as by chemically processing the sensing material [19].

Many of the ceramics/metal oxides that are used are formed by sintering at high temperatures (can be up to 1000 $^{\circ}$C). Such temperatures are too high for CMOS circuitry, making such sensors CMOS-incompatible. However, other low-temperature methods of depositing ceramics/metal oxides have been reported recently that enable CMOS-compatibility. These methods include chemical vapor deposition (CVD), sputtering, and glancing angle deposition (GLAD).

Glancing angle deposition is a very promising deposition technique for ceramics. It combines physical vapor deposition (PVD) at highly oblique vapor incidence angles with controlled substrate motion. This method enables the growth of various complex

nanostructures. The resulting films are highly porous, offer a large surface area, and have a morphology that is controllable on the 10-nm scale. The deposition conditions can be adjusted to control the film microstructure. Very high quality ceramics (in terms of humidity sensing) can be deposited using this technique. It has been used to deposit sensing materials for electrode based capacitive humidity sensors and dynamic ranges of about 1-98% have been reported. Sensitivities in the range from 0.1-30 nF/%RH and response/recovery times as low as 200 ms have been achieved [20].

Ceramics/metal oxides have very high mechanical strength, very good thermal and physical stability, are very resistant to chemical attacks. This makes them ideal candidates for harsh environment applications. They have a wide dynamic range and good sensitivity. Their response time is limited by the diffusion of the water vapor molecules. Fast response times have been obtained with certain ceramics [21]. They are not very linear. A major problem with these sensing materials is that they are very sensitive to contaminants such as dust, dirt, oil, smoke, alcohol, etc. One these impurities are sorbed, there are irreversible changes to the sensor's response. Also, when exposed to high humidity over a long time, chemisorbed hydroxyl (OH^-) ions are formed on the surface. This causes a drift in the resistance of the sensor. The hydroxyl and contaminants are usually removed using heating. Most ceramic or metal oxide humidity sensors have heaters incorporated in order to heat the sensors from time-to-time and remove all contaminants and the chemisorbed ions.

1.3.2. Porous Silicon

Porous silicon is crystalline silicon with pores or channels electrochemically etched into it to form a sponge-like material. They are formed by the anodic or galvanic etching of silicon in hydrofluoric acid. In the presence of water vapor, the vapor molecules are adsorbed and condense inside the micropores, causing a change in the electrical permittivity of the layer. They are used in electrode based capacitive humidity sensors.

Just like ceramics/metal oxides, the porosity of porous silicon and surface morphology greatly affects their humidity sensing performance. This can be controlled using additives and varying the anodisation parameters.

Sensors with porous silicon sensing layer usually have high sensitivities (up to 2700 % capacitance change [22]), but offer very poor response times (5-10 minutes). They do not suffer from thermal or humidity cycling fatigue, but do suffer from large hysteresis, and are non-linear. Also, their high reactivity causes them to be easily contaminated by the environment. Porous polysilicon can also be used as a sensing material. It offers lower sensitivity, but better response times when compared to porous silicon [23].

1.3.3. Porous Silicon Carbide

Anodisation of silicon carbide forms porous silicon carbide. Water vapor molecules are adsorbed and diffuse into its pores altering the electrical permittivity of the material. It is used in electrode based capacitive humidity sensors. The main advantage of silicon carbide is that it is very strong and resistant to harsh environments. Sensitivities of around 80% within a dynamic range of about 10-90 %RH and response time in the order of a few minutes have been reported [23]. They are usually non-linear and have a fair amount of hysteresis.

1.3.4. Polymers

A polymer is a macromolecule consisting of repeating structural units. They have a backbone made up of single, double, or triple bonded carbon atoms. Molecular or functional groups are attached to this backbone. The structure of the backbone, along with the functional groups, differentiates different polymers and their properties. Many polymers have a strong affinity for moisture. Polymers have been used for moisture sensing for a very long time. Their sensing principle is similar to that of ceramics in that the water vapor molecules are adsorbed onto their surface and diffuse/condense into the micro-pores, changing the electrical conductivity and/or permittivity of the polymer. They are used mainly in the electrode based resistive and capacitive type humidity sensors.

Since the moisture sorption causes mass changes of the polymer film, they can also be used for gravimetric humidity sensors as well as the cantilever type resistive and capacitive humidity sensors.

Polyelectrolytes and conjugated polymers are mostly used for electrode-based resistive type humidity sensors, in which the conductivity of the polymers changes with humidity. Polyelectrolytes are polymers with electrolytic groups such as salts, acids, and bases. Their backbones are hydrophobic, while the electrolytic groups are quite hydrophilic. These polymers absorb water and their conductivity increases. Polyelectrolytes are very soluble in water and this property causes deformation and loss of performance. Techniques to address this problem will be discussed shortly.

Conjugated polymers are conducting/semiconducting polymers in which single and double bonds occur alternately along the main chain. This alternation is called conjugation and gives them their conducting/semiconducting property. Despite this, they are still not very conductive due to lack of charge carriers. The conductivity can be increased by doping. When water is absorbed, it releases protons (protonation) which interacts with the conjugated double bonds. This effect is used for humidity sensing. The conductivity varies as water is absorbed and dopants can be used to control this variation. Conjugated polymers are usually hydrophobic and are not able to absorb much water. Hence, their sensitivities are usually low. However, they can be combined with hygroscopic polymers to enhance their response.

The types of polymers used for electrode-based capacitive humidity sensing usually include hydrophobic materials with a bit of hygroscopicity. The hygroscopic nature is required to attract water vapor. These type of polymers are both non-ionic and high polar. Examples of such polymers include esters and polyimide. Humidity response of these types of polymers is very high linear. They usually suffer from hysteresis due to clustering of water molecules inside the polymer, but this depends on the type of polymer used. This clustering effect can be reduced using cross-linking. Cross-linking also increases the sensitivity sometimes depending on the cross-linking reagent.

Some polymers, mainly polyelectrolytes, are very soluble in water. This causes them to degrade or lose performance in high humidity or dew forming atmospheres. Due to their high solubility, their conductivity reaches a very high value at low humidity values. This causes their high humidity response to be weak. For these types of polymers, humidity switching usually lowers their performance and life time. There are various methods to address these problems.

- Cross-linking: this involves forming a sort of bridge between two polymer chains in order to create a dense, insoluble, and intensive polymer network.

- Interpenetrating polymer network (IPN): this consists of a cross-linked polyelectrolyte (or hydrophilic polymer) and a cross-linked hydrophobic polymer combined together such that they interlock or interpenetrate each other. This forms an even more intensive polymer network with higher insolubility and lifetime.

- Graft-polymerization: This involves attaching or grafting atoms or groups to the main backbone of the polymer at different points. This makes the polymer more resistive to water. Also, by adding some insulating content, the conductivity at low humidity is reduced, hence increasing the sensitivity at high humidity.

- Co-polymerization: this is a process in which a polymer is chemically synthesized from two or more monomers.

Most of these techniques can be combined with each other. For example, the formation of an interpenetrating polymer network with a cross-linked copolymer and a cross-linked hydrophobic polymer. Using these techniques to form strong, insoluble, and long-lasting polymers for humidity sensing is a huge part of literature [24-31].

1.3.5. Carbon Nanotubes (CNTs)

These are cylindrical carbon molecules with outstanding mechanical, thermal, chemical, and electrical properties. They are about a 100 times stronger than steel and maintain very high current densities. Their thermal conductivity is comparable to that of diamond. Carbon nanotubes are usually few nanometers in diameter and can be several micrometers long. There are two types: single-walled carbon nanotubes (SWCNTs) and multi-walled carbon nanotubes (MWCNTs). They form a porous-like nanostructure offering very high surface area enabling high-resolution humidity sensing via adsorption of water vapor molecules. Capillary condensation is induced in the micropores at low humidity levels, hence amplifying capacitive response. They can be used in capacitive, resistive, and gravimetric humidity sensors. The best QCM humidity sensor performance reported was obtained using CNTs as the sensing layer [5].

The conductivity change with humidity is fairly linear [12], but the capacitive change with humidity is not linear [32]. Response times range from a few second to tens of seconds. Capacitive humidity sensors using CNTs showed sensitivities up to 3700 % at high humidity [32].

1.4. Main Contributions of this Work

- In this work, electrode-based, stack-structure, capacitive relative humidity sensors, with a thin polymer film as the sensing layer, were designed and fabricated to demonstrate highly linear, high sensitivity and fast humidity sensing using MEMS.

- A MATLAB simulation model, based on the mathematics of moisture adsorption and diffusion, was developed for simulating the dynamic response of the sensors.

- The MATLAB simulation model, as well as CoventorWare (for steady-state simulations), were used to show how a specific sensor design can be optimized for performance and how sensors of different structures and geometries compare with each other.

- With CMOS compatibility being a major requirement for this work, a microfabrication process flow that has a low thermal budget (≤ 300 °C), as well as material and chemical compatibility with CMOS IC fabrication was developed and optimized.

    - Published IEEE paper:
      P. V. Cicek, T. Saha, B. Waguih, F. Nabki, and M. N. El-Gamal, "*Design of a Low-Cost MEMS Monolithically-Integrated Relative Humidity Sensor*", International Conference on Microelectronics, pp. 172, 2010.

- The capability to shield the sensor from humidity in order to have a reference device was developed and optimized – it provides a reference value enabling more accurate capacitance measurements using electronic circuits and also provides a means of temperature compensation without the need for a high resolution temperature sensor, and integrated heater, or a temperature insensitive clock.

    - Published IEEE paper:
      K. Allidina, T. Saha, and M. N. El-Gamal, "*A Temperature Compensated Architecture for Integrated, Low Power, Frequency Domain Sensor*", International Conference on Microelectronics, pp. 164-167, 2010.

- The sensing polymer layer forms the most crucial part of the sensor and determines the overall performance. A very low cost, simple, robust, repeatable, and reliable technique to deposit very thin, low stress, highly planar, high quality polymer layers was developed and optimized.

- A very convenient, reliable, and versatile technique was reported and used for fabricating the MEMS sensors on top of CMOS IC dies of any size to demonstrate the capability of full monolithic integration of MEMS and IC.

  - IEEE paper in preparation:
    P. V. Cicek, Q. Zhang, T. Saha, S. Mahdavi, K. Allidina, F. Nabki, and M. N. El-Gamal, "*A Novel Prototyping Method for Die-Level Monolithic Integration of MEMS Above-IC*", Journal of Micromechanics and Microengineering (IOP Science), 2012 – in review.

- A novel, robust, and accurate response time test setup, using thin latex membranes, was designed for testing the behavior of the sensors when exposed to relative humidity steps and obtaining the response time of the sensors.

1.5. References

[1] "MEMS/NEMS Handbook: Techniques and Applications", vol. 4, Sensors and Actuators.

[2] D. H. Lee, H. K. Hong, C. K. Park, G. H. Kim, Y. S. Jeon, and J. U. Bu, "A Micromachined robust humidity sensor for harsh environment applications", *Micro Electro Mechanical Systems*, pp. 558-561, 2001.

[3] B. Okcan and T. Akin, "A Low-Power Robust Humidity Sensor in a Standard CMOS Process", *Electron Devices*, vol. 54, pp. 3071-3078, Nov. 2007.

[4] Z. Fang, Z. Zhao, Y. Wu, B. Zhang, and Y. Wang, "Integrated temperature and humidity sensor based MEMS", *Information Acquisition*, pp. 84-87, June 2004.

[5] K. Jaruwongrungsee, A. Wisitsoraat, A. Tuantranont, and T. Lomas, "Humidity sensor utilizing multiwalled carbon nanotubes coated quartz crystal microbalance", *Nanoelectronics Conference*, pp. 961-964, March 2008.

[6] E. Radeva, V. Georgiev, L. Spassov, N. Koprinarov, and St. Kanev, “Humidity adsorptive properties of thin fullerene layers studies by means of quartz micro-balance”, *Sensors and Actuators B*, vol. 42, pp. 11-13, 1997.

[7] T. Nomura, K. Oofuchi, T. Yasuda, and S. Furukawa, “SAW humidity sensor using dielectric hygroscopic polymer film”, *Ultrasonics Symposium*, vol. 1, pp. 503-506, Nov. 1994.

[8] A. Kawalec and M. Pastemack, “A New High-Frequency Surface Acoustic Wave Sensor for Humidity Measurement”, *Instrumentation and Measurement*, vol. 57, pp. 2019-2033, Sep. 2008.

[9] A. Gluck, W. Halder, G. Lindner, H. Muller, and P. Weindler, “PVDF-excited Resonance Sensors for Gas Flow and Humidity Measurements”, *Sensors and Actuators B*, pp. 554-557, 1994.

[10] L. T. Chen, C. Y. Lee, and W. H. Cheng, “MEMS-based humidity sensor with integrated temperature compensation mechanism”, *Sensors and Actuators A*, vol. 147, pp. 552-528, Oct. 2008.

[11] K. I. Arshak and K. Twomey, “Investigation into a novel humidity sensor operating at room temperature”, *Microelectronics Journal*, vol. 33, pp. 213-220, March 2002.

[12] L. Liu, X. Ye, K. Wu, R. Han, Z. Zhou, and T. Cui, “Humidity Sensitivity of Multi-Walled Carbon Nanotube Networks Deposited by Dielectrophoresis”, *Sensors*, Vol. 9, pp. 1714-1721, 2009.

[13] M. Packirisamy, I. Stiharu, X. Li, and G. Rinaldi, “A polyimide based resistive humidity sensor”, *Sensor Review*, Vol. 25, pp. 271-276, 2005.

[14] M. J. Lee, C. Lee, V. R. Singh, K. Yoo, and N. Min, “Humidity sensing characteristics of plasma functionalized multiwall carbon nanotube-Polyimide composite films”, *Sensors*, pp. 430-433, Oct. 2008.

[15] C. Y. Lee and G. B. Lee, “Micromachine-based humidity sensors with integrated temperature sensors for signal drift compensation”, *Journal of Micromechanics and Microengineering*, pp. 620-627, 2003.

[16] C. Dai, “A capacitive humidity sensor integrated with micro heater and ring oscillator circuit fabricated by CMOS–MEMS technique”, *Sensors and Actuators B*, Vol. 122, pp. 375-380, 2007.

[17] J. S. Kim, K. Kwak, K. Kwon, N. Min, and M. Kang, “A locally cured polyimide-based humidity sensor with high sensitivity and high speed”, *Sensors*, pp. 434-437, Oct. 2008.

[18] W. Yingcai and G. Zhengtian, “Metal-Insulator-Semiconductor BaTiO3 Humidity Sensor”, *Photonics and Optoelectronics*, pp. 1-4, Aug. 2009.

[19] F. Hossein-Babaei and S. Rahbarpour, “Porosity modification for the adjustment of the dynamic range of ceramic humidity sensors”, *Sensing Technology*, pp. 648-651, Dec. 2008.

[20] M. R. Kupsta, M. T. Taschuk, M. J. Brett, and J. C. Sit, “Reative Ion Etching of Columnar Nanostructured TiO_2 Thin Films for Modified Relative Humidity Sensor Response Time”, *Sensors Journal*, vol. 9, pp. 1979-1986, Dec. 2009.

[21] E. Traversa, “Ceramic sensors for humidity detection: the state-of-the-art and future developments”, *Sensors and Actuators B*, Vol. 23, pp. 135-156, Feb. 1995.

[22] G. M. Halloran, M. Kuhl, P. J. Trimp, and P. J. French, “The effect of additives on the adsorption properties of porous silicon, *Sensors and Actuators*, Vol. 61, pp. 415-420, June 1997.

[23] E. J. Connolly, P. J. French, H. T. M. Pham, and P. M. Sarro, “Relative humidity sensors based on porous polysilicon and porous silicon carbide”, *Sensors*, Vol. 1, pp. 499-502, 2002.

[24] Y. Sakai, Y. Sadaoka, and M. Matsuguchi, “Humidity sensors based on polymer thin films”, *Sensors and Actuators B*, Vol. 35, pp. 85-90, Sep. 1996.

[25] Y. Li, Y. Chen, C. Zhang, T. Xue, and M. Yang, “A humidity sensor based on interpenetrating polymer network prepared from poly(dimethylaminoethyl methacrylate) and poly(glycidyl methacrylate)”, *Sensors and Actuators B*, Vol. 125, pp. 131-137, July 2007.

[26] Y. Sakai, Y. Sadaoka, M. Matsuguchi, and H. Sakai, “Humidity sensor durable at high humidity using simultaneously crosslinked and quaternized poly (chloromethyl styrene)”, *Sensors and Actuators B*, Vol. 25, pp. 689-691, April 1995.

[27] C. Roman, O. Bodea, N. Prodan, A. Levi, E. Cordos, and I. Manoviciu, “A capacitive-type humidity sensor using crosslinked poly(methyl methacrylate-co-(2 hydroxypropyl)-methacrylate)”, *Sensors and Actuators B*, Vol. 25, pp. 710-713, April 1995.

[28] M. Matsuguch, T. Kuroiwa, T. Miyagishi, S. Suzuki, T. Ogura, and Y. Sakai, “Stability and reliability of capacitive-type relative humidity sensors using crosslinked polyimide films”, *Sensors and Actuators B*, Vol. 52, pp. 53-57, Sep. 1998.

[29] Y. Sakai, “Humidity sensors using chemically modified polymeric materials”, *Sensors and Actuators B*, Vol. 13, pp. 82-85, May 1993.

[30] B. Adhikari and S. Majumdar, “Polymers in Sensor Applications”, *Progress in Polymer Science*, Vol. 29, pp. 699-766, July 2004.

[31] M. Matsuguchi, Y. Sadaoka, Y. Nuwa, M. Shinmoto, and Y. Sakai, “Capacitive-type humidity sensors using polymerized vinyl carboxylate”, *Journal of the Electrochemical Society*, Vol. 141, pp. 614-618, 1994.

[32] J. T. W. Yeow and J. P. M. She, “Carbon nanotube-enhanced capillary condensation for a capacitive humidity sensor”, *Nanotechnology*, Vol. 17, No. 21, Oct. 2006.

[33] Z. Chen and C. Lu, “Humidity Sensors: A review of Materials and Mechanisms”, *Sensor Letters*, Vol. 3, pp. 274-295, 2005.

[34] F. Nabki, K. Allidina, F. Ahmad, P. V. Cicek, and M. N. El-Gamal, “A highly integrated 1.8 GHz frequency synthesizer based on a MEMS resonator”, *Journal of Solid State Circuits*, Vol. 44, pp. 2154-2168, 2009.

[35] J. J. Steele, J. P. Gospodyn, J. C. Sit, and M. J. Brett, “Impact of morphology on high-speed humidity sensor performance”, *Sensors Journal*, Vol. 6, pp. 24-27, 2006.

[36] J. Seetharamappa, S. Yellappa, and F. D’Souza, “Carbon Nanotubes: Next Generation of Electronic Materials”, *The Electrochemical Society*, 2006.

2. Design/Simulation

2.1. Sensor Type and Sensing Material

As discussed in chapter 1, there are several different types of relative humidity sensors and a whole multitude of materials that can be used for humidity sensing. The first step in the design process is to select a certain type of sensor and the sensing material to be used. In this work, no specific application or set of specifications were being targeted. The goal was to design a relative humidity sensor that can be used for most applications with reasonable specifications.

Sensor Type – Electrode based capacitive type relative humidity sensor was chosen for the following reasons:

- High linearity
- Wide humidity measuring range
- Mechanical resilience – the device structure is simple with no moving parts. Hence, the fabrication yield can be high and device failure rate is low.
- Reasonable complexity of interface circuitry – measuring capacitive changes is common and can be done accurately with different circuit configurations.
- Low power consumption – there is no power consumption at DC, which is very beneficial from an overall system and industrial perspectives.

Sensing Material - Capacitive humidity sensors can use a whole variety of sensing materials. A special type of polymer was chosen as the sensing material due to the following reasons:

- High linearity
- Low hysteresis
- High sensitivity
- Resistance to most chemicals

- Compatibility with integrated circuit (IC) fabrication
- High thermal stability
- Relatively easy to prepare and deposit
- Readily available

This polymer is non-ionic, but highly polar. This gives it both hygroscopic and hydrophobic properties. The hygroscopicity enables it to attract and sense water vapor molecules, while the hydrophobic nature is essential for preventing performance drop or dissolution of the polymer in high humidity or dew-forming environments.

Both the electrode based capacitive type humidity sensor and the polymer sensing material allow for a CMOS-compatible fabrication process, enabling total system integration, which is a key component of this work. This also implies that the parasitic effects will be reduced since the sensing device and the interface circuits will be on the same substrate. There will be no interconnect parasitics like those present in conventional solutions and this will serve to maximize the sensitivity.

2.2. Structure and Geometry

Once the sensing layer has been chosen, the next phase is to design the structure and geometry of the capacitive sensing device. For electrode based capacitive sensors, there are two types possible – stack structure and lateral structure. The lateral structure provides lower capacitances and generally has lower sensitivities. Hence, in this work, the stack structure device was implemented. This basically consists of a stack of metal-polymer-metal. It’s a simple parallel plate capacitor with polymer as the dielectric sandwiched between two metal electrodes.

The top electrode cannot be completely flat since there will be no exposure of the polymer underneath to ambient moisture. Some metals are moisture permeable and hence can be completely flat and still allowing for moisture to diffuse into the polymer below.

However, only a few metals are moisture permeable (e.g. gold) and they have to be quite thin (<100nm preferably). This imposes a strict restriction on the fabrication process flow. The other disadvantage is that the response time will be high since the moisture first has to diffuse through the metal before getting into the polymer - there is no direct exposure of the polymer to the ambient humidity. Due to these disadvantages, the top electrode needs to be patterned in order to provide direct exposure of the polymer to moisture. In this work, this was done in two ways: Design-A, in which the top electrode was patterned as rectangular fingers and Design-B, in which the top electrode was patterned with square holes. Both structures are shown in Fig. 1-2.

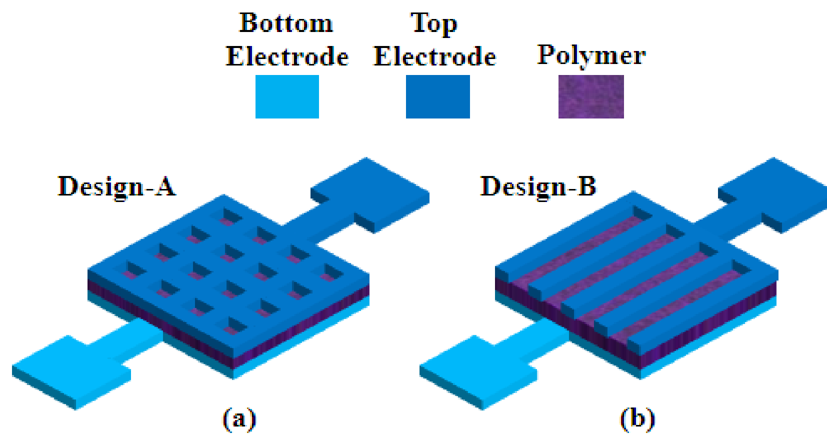

Figure 1-2: Capacitive humidity sensing devices - (a) Design-A: top electrode with square holes and (b) Design-B: top electrode as rectangular fingers

In both designs, there are openings in the top electrode so that there is direct contact of the polymer with the ambient air. This allows for humidity diffusion into the polymer film underneath the top electrode. The cross-section of both design types can be represented using the diagram shown in Fig. 2-2.

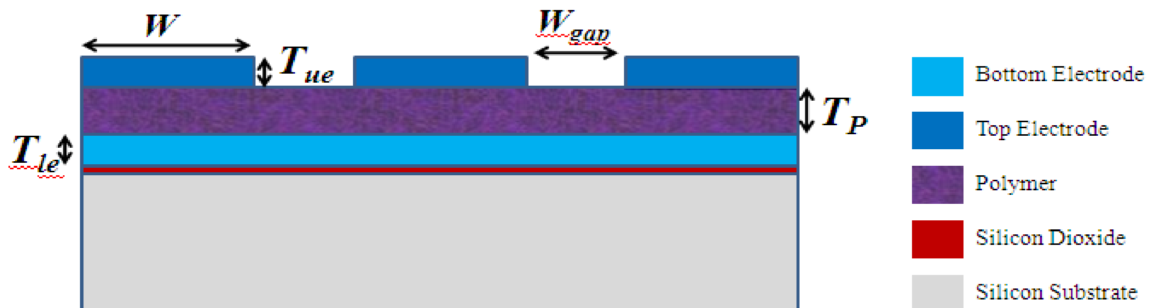

Figure 2-2: Cross-section of the capacitive humidity sensor

W_{gap} represents the spacing between the fingers in Design-A and the width of the holes in Design-B. W is the width of the fingers in Design-A and the spacing between the holes (or the width of the top metal) in Design-B. T_{ue} is the thickness of the top electrode, T_{le} is the thickness of the bottom electrode, and T_P is the thickness of the polymer. Once the structure has been decided on, the geometry needs to be designed (i.e. the values of W, W_{gap}, T_{ue}, T_{PI}, and T_{le} needs to be optimized). This can be done on the basis of two main design criteria.

The first design criterion is to maximize the area of contact between the sensing layer and the ambient air, and to have the shortest pathway to vapor absorption to all points in the polymer. This will serve to minimize the response time of the sensor. The response time is dependent on the largest distance (L) required for the moisture to reach all points within the sensing material. Response time obeys Fick's law and can be expressed as:

$$t_{resp} \propto \frac{L^2}{D} \quad \ldots\ldots\ldots (5)$$

D is the humidity diffusion constant and is set by the sensing material. The only degree of freedom is L. The geometry of the sensor device is optimized to minimize L and allow for fast diffusion to all points within the sensing film.

With Fick's law in mind, the polymer thickness, T_P, and the top electrode width, W, needs to be as small as possible to allow for fast diffusion of moisture to all points within the polymer. If T_P is large, it takes more time for moisture to diffuse vertically into the polymer. If W is large, it takes more time for moisture to diffuse laterally into the polymer under the top electrode. Both cases imply large response time. Hence, for fastest response time, both variables need to be made as small as allowed by the design technology. However, if $W >> L$, the response time will be dominated by the time it takes for moisture to diffuse laterally through W, since the vertical diffusion time through L will be much smaller and will have a negligible effect on the overall response time, which consists of both the horizontal and vertical diffusion occurring simultaneously.

The second design criterion is to minimize parasitic fringing capacitances. The sensitivity of the sensor is dependent on parasitics according to the following relation:

$$S \propto \frac{\Delta C / C_{0\,active}}{1 + \frac{C_{0\,parasitic}}{C_{0\,active}}} \quad \ldots\ldots\ldots(6)$$

In (6), S is the sensitivity, $C_{0active}$ is the nominal active capacitance of the sensor that is affected by relative humidity changes, and $C_{0parasitic}$ is the nominal parasitic capacitance that is independent of relative humidity. From this relationship, it is clear that the parasitics need to be reduced in order to maximize sensitivity. This can be achieved through the careful design of the sensor geometry. All the design parameters, T_{le}, T_{ue}, T_P, W, and W_{gap}, influence $C_{0active}$ and $C_{0parasitic}$, and hence will contribute to the overall sensitivity of the sensor. The patterning of the bottom electrode also affects the sensitivity. These will be discussed in more detail using simulation results in the next section.

2.3. Simulation

2.3.1. Steady-State Simulations (CoventorWare)

The Clausius-Mossotti equation (7) relates the macroscopic and microscopic characteristics of dielectrics.

$$\sum_i N_i \alpha_i = 3\varepsilon_0 \frac{\varepsilon(RH) - 1}{\varepsilon(RH) + 2} \quad \ldots\ldots\ldots(7)$$

In (7), N is the number of dipoles per unit volume, α is the molecular polarizability, ε_0 is the permittivity of free space, and ε(RH) is the permittivity of the dielectric at the given relative humidity. For the given polymer-water system, the difference between (Nα) at 0 %RH and (Nα) at a given RH can be attributed to the moisture absorbed by the polymer as a result of the relative humidity change. Applying this to (7) gives a variant of the

Clausius-Mossotti equation (8), which can be used to relate the permittivity of polymer to the amount of moisture in the polymer [4].

$$(N\alpha)_{H_2O} = 3\varepsilon_0 \left[\left(\frac{\varepsilon(RH) - 1}{\varepsilon(RH) + 2} \right) - \left(\frac{\varepsilon(0\ \%RH) - 1}{\varepsilon(0\ \%RH) + 2} \right) \right] \quad \ldots\ldots\ldots (8)$$

This equation can be used to calculate the permittivity of the polymer for different amounts of water absorbed as a result of relative humidity changes. From the product datasheet of the polymer used and other general physical, thermal, electrical, and chemical properties of the polymer, the electrical permittivity change of the polymer from 0 to 100 %RH was calculated using (8).

Permittivity Change of the Polymer (over 100 %RH at Room Temperature): 2.9 to 3.7

Using this permittivity variation, steady-state sensitivity simulations were carried out using CoventorWare, which is a design and simulation software for MEMS. Both Design-A (top electrode patterned as rectangular fingers) and Design-B (top electrode patterned with square holes) were modeled in CoventorWare and simulations were carried out to study the sensitivity difference between both designs and to study the dependence of sensor sensitivity on the bottom electrode thickness (T_{le}), top electrode thickness (T_{ue}), polymer thickness (T_P), top electrode width (W), and spacing of top electrode or width of top electrode opening (W_{gap}).

Design-A Sensitivity vs. Design-B Sensitivity / Sensor Sensitivity vs. Top Electrode Thickness (T_{ue})

The thickness of the top electrode (T_{ue}) was varied and the sensitivity for each thickness was recorded. Fig. 3-2 shows the simulation results for both Design-A and Design-B. Sensitivity was measured as the total sensor capacitance variation from 0 %RH to 100 %RH (i.e. capacitance variation from ε = 2.9 to ε = 3.7).

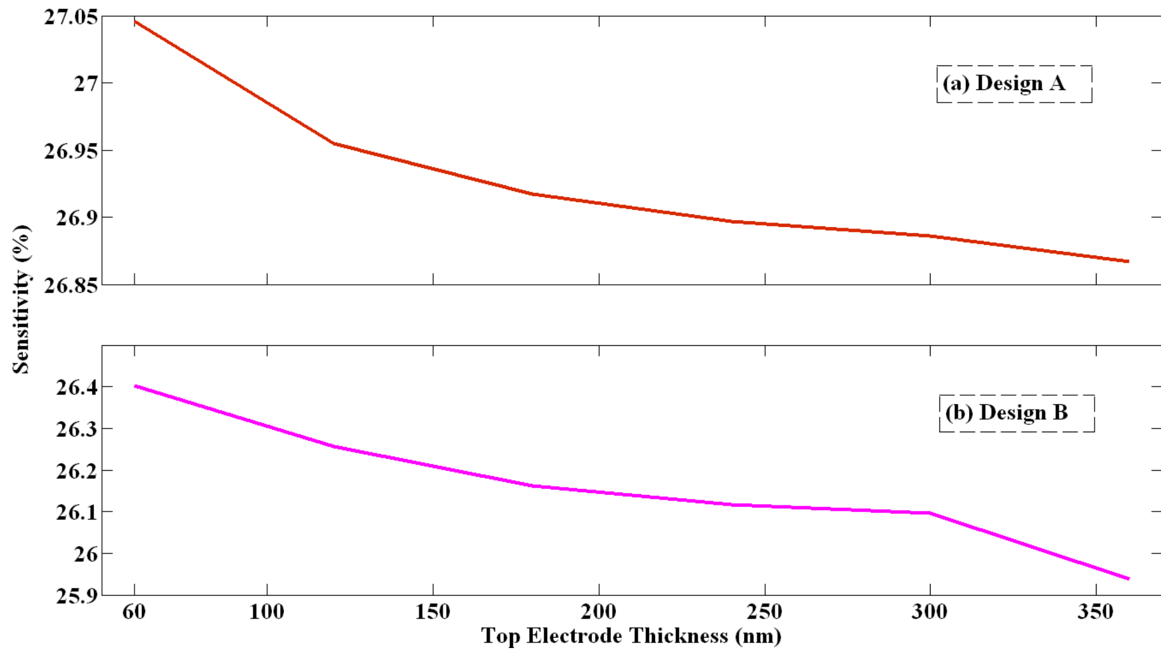

Figure 3-2: Plot of sensor sensitivity against its top electrode thickness for (a) Design-A and (b) Design-B

Fig. 3-2 -- firstly, it can be seen that the sensitivity of Design-A is higher than that of Design-B. This can be explained as follows - the parasitic portion of the nominal sensor capacitance serves to decrease the sensitivity as explained earlier (6). This parasitic portion increases if there are more electric field lines in air, since the permittivity of air is unaffected by humidity. In both designs, there is air present in the top metal openings (in the volume defined by W_{gap}) and field lines in these regions serve to introduce parasitic fringing capacitance. In Design-A, the total air volume in which fringing field lines are present is smaller (by about 45 %) than in Design-B. Also, Design-A has a lower total top electrode perimeter (lower by about 4%) than Design-B, which means less fringing fields. In other words, Design-B has a larger total air volume in which fringing field lines are present and an increased amount of fringing fields, both of which imply a higher fringing field or parasitic capacitance, and hence lower sensitivity.

Fig. 3-2 – secondly, it shows that the sensitivity of both design types slightly decreases as the top electrode thickness increases. This can be explained as follows - for thicker metals, there are more fringing field lines in air, which serves to increase the parasitic portion of the nominal sensor capacitance, but the active capacitance remains the same. As a result, the sensitivity decreases as top electrode thickness increases.

Sensor Sensitivity vs. Polymer Thickness (T_P)

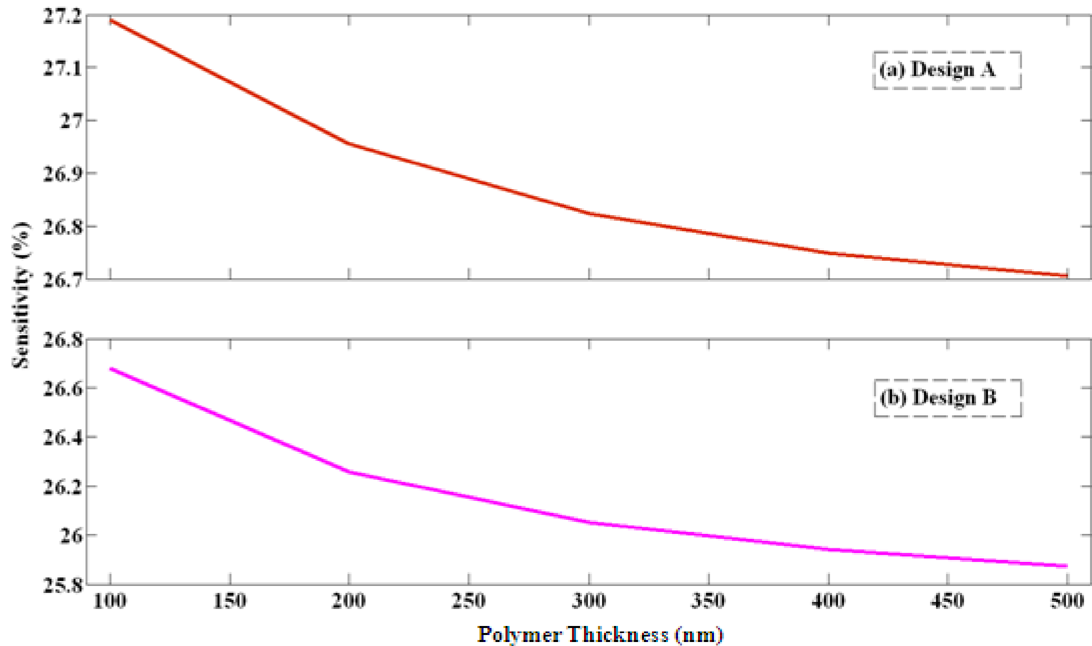

Figure 4-2: Plot of sensor sensitivity against its polymer thickness for (a) Design-A and (b) Design-B

The polymer thickness (T_P) was varied and the sensitivity for each thickness was recorded. Fig. 4-2 shows the simulation results for both Design-A and Design-B. As can be seen, the sensitivity of both design types decreases as the polymer thickness increases. This can be explained as follows - for thinner polymer layers, the active capacitance is increased more than the fringing parasitic capacitance, and hence the sensitivity increases as polymer thickness decreases.

Sensor Sensitivity vs. Top Electrode Width (W)

The top electrode width (W) was varied and the sensitivity for each width was recorded. Fig. 5-2 shows the simulation results for both Design-A and Design-B. As can be seen, the sensitivity of both design types increases as the top electrode width increases. This can be explained as follows – for larger top electrode widths, the active capacitance is increased with no change in fringing parasitic capacitance. This results in larger sensitivity.

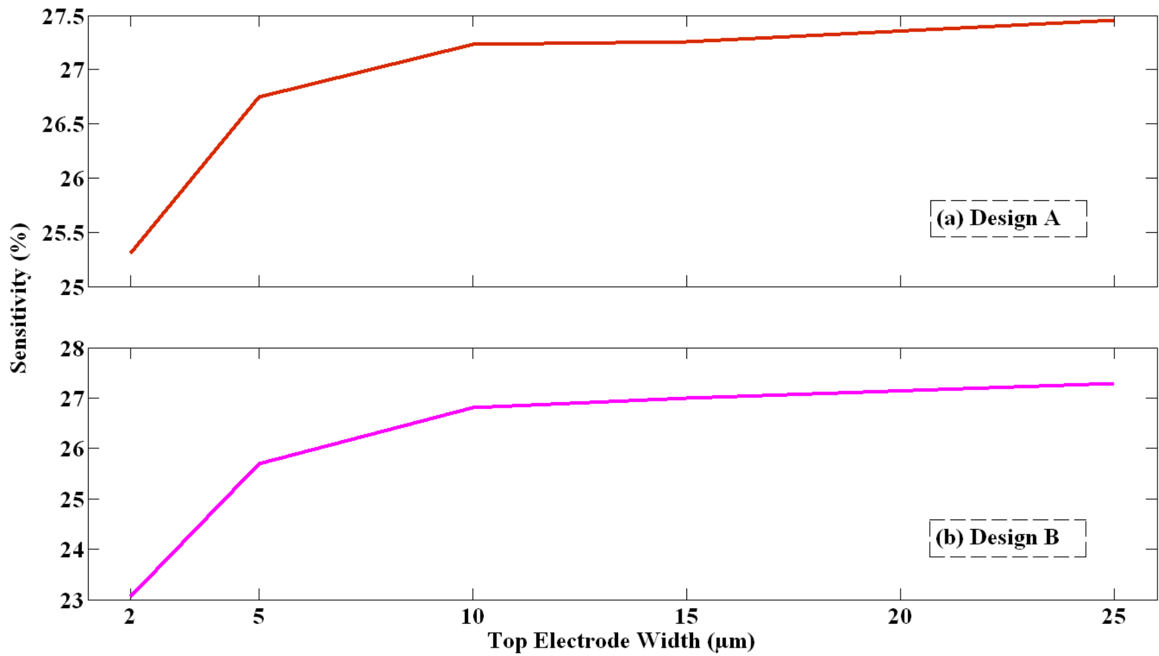

Figure 5-2: Plot of sensor sensitivity against the top electrode width for (a) Design-A and (b) Design-B

Sensor Sensitivity vs. Top Electrode Gap/Spacing (W_{gap})

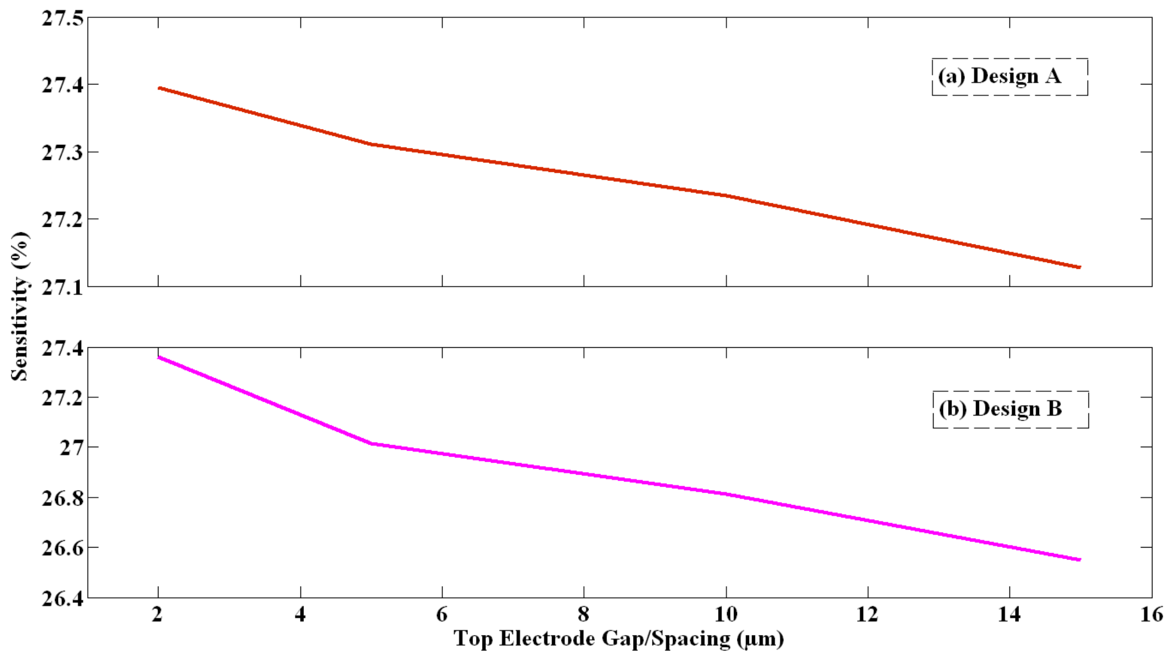

Figure 6-2: Plot of sensor sensitivity against the top electrode gap for (a) Design-A and (b) Design-B

The top electrode gap width (W_{gap}) was varied and the sensitivity for each width was recorded. Fig. 6-2 shows the simulation results for both Design-A and Design-B. As can be seen, the sensitivity of both design types decreases as the top electrode gap increases.

This can be explained as follows – for larger top electrode gaps, the active capacitance remains the same, but the air regions, in which fringing fields are present, are larger, and hence the parasitic fringing capacitance is larger. This worsens the sensitivity.

Flat vs. Patterned Bottom Electrode / Sensor Sensitivity vs. Bottom Electrode Thickness (T_{le})

Both Design-A and B have a flat bottom electrode and a patterned top electrode. The top electrode is patterned to expose the polymer to moisture. There is no need to pattern the bottom electrode. However, it was noticed from CoventorWare simulations that patterning the bottom electrode to be identical to the top electrode increases the sensor sensitivity. **The sensitivity of Design-A increases by about 1 %, while that of Design-B increases by 2.5 %.**

The increase in sensitivity can be attributed to the decrease in fringing parasitic capacitance. Patterning the bottom electrode reduces the field lines since there is less electrode area. The fringing fields are reduced and hence, the parasitic fringing capacitance is reduced. This serves to increase the overall sensitivity of the sensor. However, the increase in sensitivity is higher for Design-B devices than for Design-A devices. This is due to the fact that the patterning of the bottom electrode reduces the bottom electrode area more in Design-B than in Design-A, and hence the reduction in fringing field lines will be more in Design-B than in Design-A. As a result, the reduction in parasitic capacitance, and the corresponding increase in sensitivity, due to bottom electrode patterning, is less in Design-A than in Design-B.

Varying the bottom electrode thickness affects the sensitivity. Fig. 7-2 shows the simulation results. As can be seen, the sensitivity decreases with increasing bottom electrode thickness. This can be attributed to the fact that fringing fields from the bottom electrode increases as its thickness increases and also, the air volume depth in the top metal openings increases as the bottom electrode thickness increases. This increases

parasitic capacitance, and hence reduces sensitivity. Fig. 8-2 shows how a thicker bottom electrode results in a larger air volume in which field lines are present.

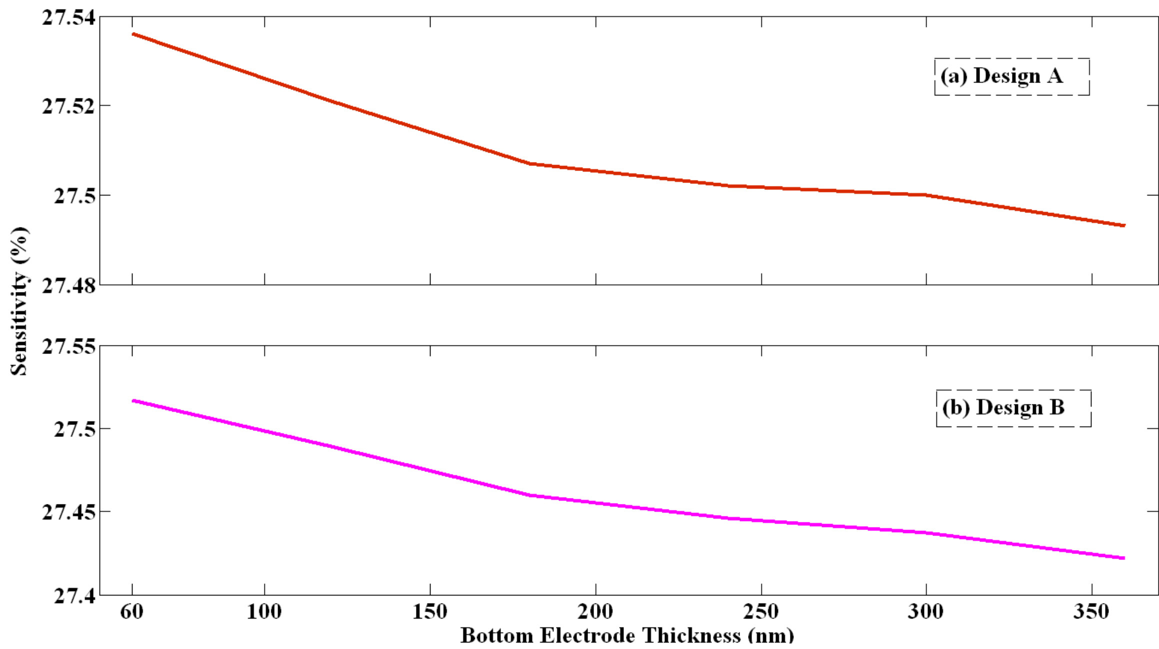

Figure 7-2: Plot of sensor sensitivity against the thickness of the patterned bottom electrode for (a) Design-A and (b) Design-B

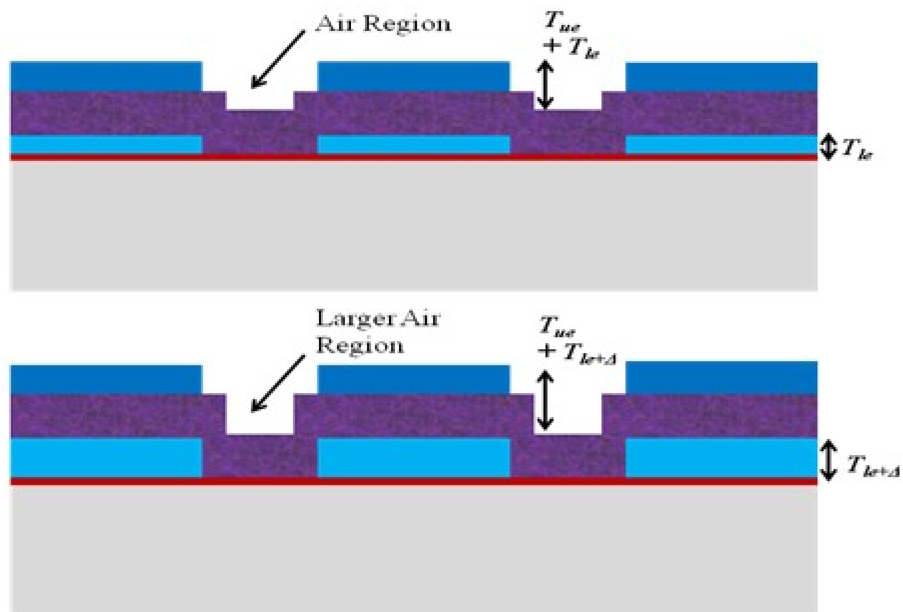

Figure 8-2: Cross-section diagram indicating larger air region for fringing fields due to patterned bottom electrode

These simulations are very useful for optimizing designs and comparing the performance of different designs with each other. They may not however provide the correct absolute sensitivity values. The simulations are based on certain theoretical values such as the total moisture absorption of the polymer and the calculated values of the dielectric constant of the polymer at 0 and 100 %RH. These values may be different for the actual devices. Finally, for practical measurements, the variation of the dielectric constant of the polymer with humidity depends on the measuring test frequency, which is not the case in simulations.

2.3.2. Dynamic Simulations (MATLAB Simulation Model)

A MATLAB simulation model was developed to study the dynamic response of the sensors - specifically to study the response of the sensors to abrupt humidity changes (humidity steps) and measure the response time. The theory behind moisture adsorption and diffusion, as well as the MATLAB model are described at the end of the chapter. This section discusses the simulation results obtained using the simulation model.

Simulation Results

The response time of the sensor is defined by the time it takes for the moisture to reach all areas of the polymer, mainly the areas underneath the top metal since this is what defines the active capacitance of the sensor. This time is mainly dependent on the thickness of the polymer, T_P (which sets the vertical diffusion time) and the width of the top metal, W (which sets the lateral diffusion time). The width of the openings in the top metal (W_{gap}), and the thickness of both the top and bottom electrodes (T_{ue} and T_{le}) do not influence the response time in a significant manner. This is because these parameters do not significantly affect the time it takes for the moisture to diffuse both laterally and vertically in the polymer.

The response of the sensors to a relative humidity step was simulated and the normalized sensor capacitance change was plotted against time. The results are summarized below.

Both Designs-A and B were simulated for a 25%RH step and for $W = W_{gap} = 5$ µm. Fig. 9-2 shows the normalized change in capacitance of both designs against time. As can be seen, both designs have an identical response since the vertical polymer thickness and most importantly, the lateral polymer thickness which moisture has to diffuse through (i.e. the metal width W) is the same for both. From the experimental results shown in chapter 3, it will be seen that the two designs show a difference in their response times. This is simply because the effective diffusion constant in reality varies with the moisture concentration profile, whereas the simulation model is based on Fick's diffusion law which is solved assuming diffusion constant that remains the same throughout the moisture diffusion.

The response variation as the top metal width W is increased (i.e. as the lateral distance the moisture has to diffuse through is increased) is shown in Fig. 10-2. From this, it can be seen that the response time increases as W is made larger. This is expected since a larger W corresponds to a larger lateral distance the moisture has to diffuse through in the polymer underneath the top metal, and this implies a longer time for the moisture to reach all regions of the polymer. The response time can be defined as the time it takes for the sensor to reach 63% ($-$) of its final change. The response time values are shown in Table 1-2.

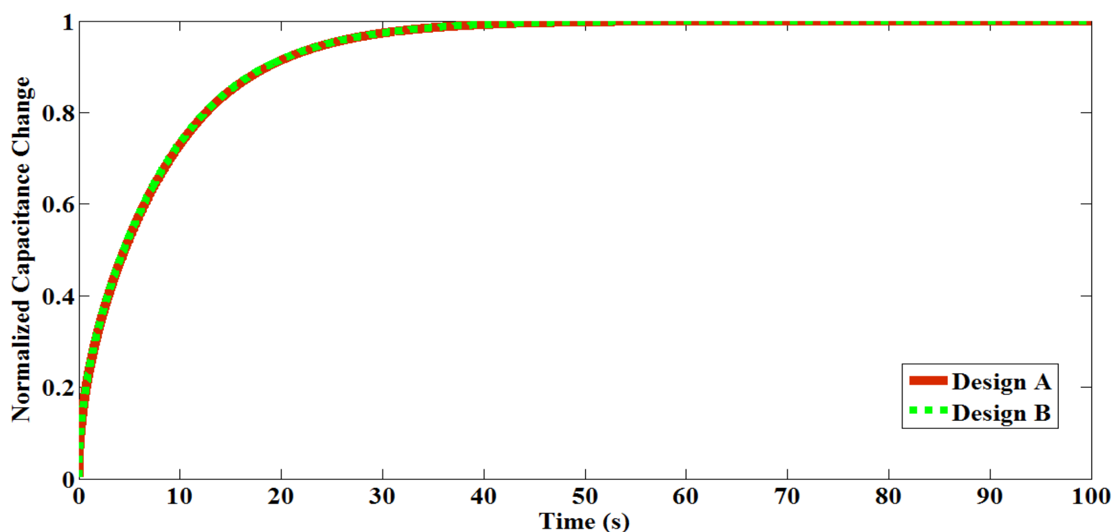

Figure 9-2: Normalized capacitance change for Designs-A and B for a 25 %RH step

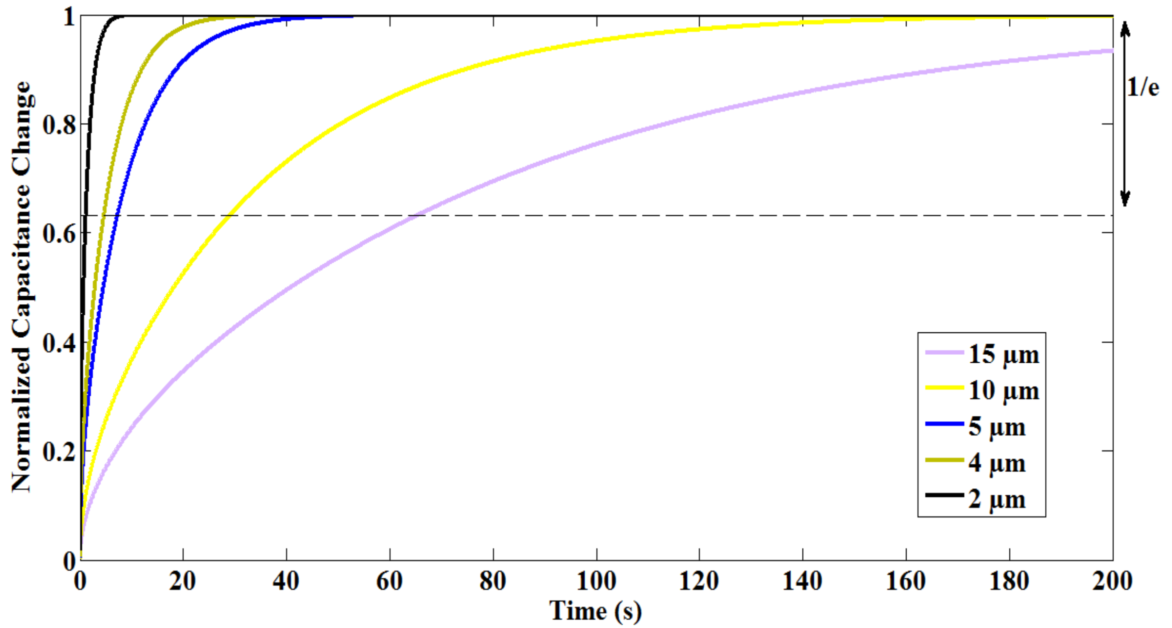

Figure 10-2: Response variation as top metal width (W) is increased

W (µm)	Response Time (s)
2	**1.1**
4	**4.6**
5	**7.2**
10	**28.9**
15	**64.9**

Table 1-2: Response time corresponding to the various top metal widths (W)

As mentioned earlier, the response time is also dependent on the thickness of the polymer. The response time increases for thicker polymer layers. However, in this work, the polymer thicknesses used were much smaller than the minimum top metal width. Due to this, the response time is dominated by the lateral diffusion time controlled by the top metal width (W), while the vertical diffusion time controlled by the polymer thickness (T_P) is insignificant to the overall response.

2.4. Process Flow

The microfabrication process flow designed to fabricate the humidity sensors in the McGill Microfabrication Facility is shown below.

- **Starting Material**

  (Silicon wafer with thermal oxide coating)

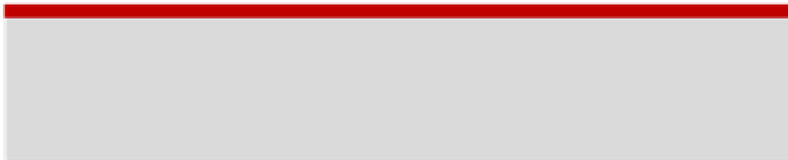

a) Sputter aluminum (bottom electrode)

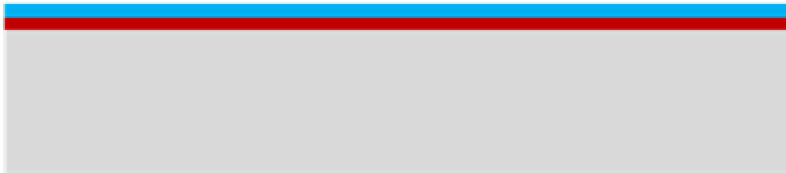

b) Pattern aluminum using Mask 1

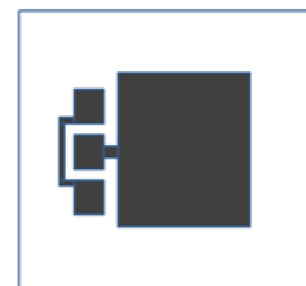

Mask 1

c) Spin-coat and cure the polymer

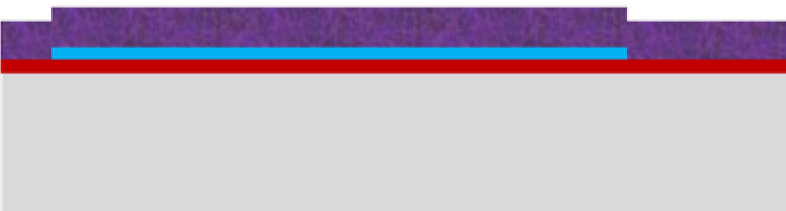

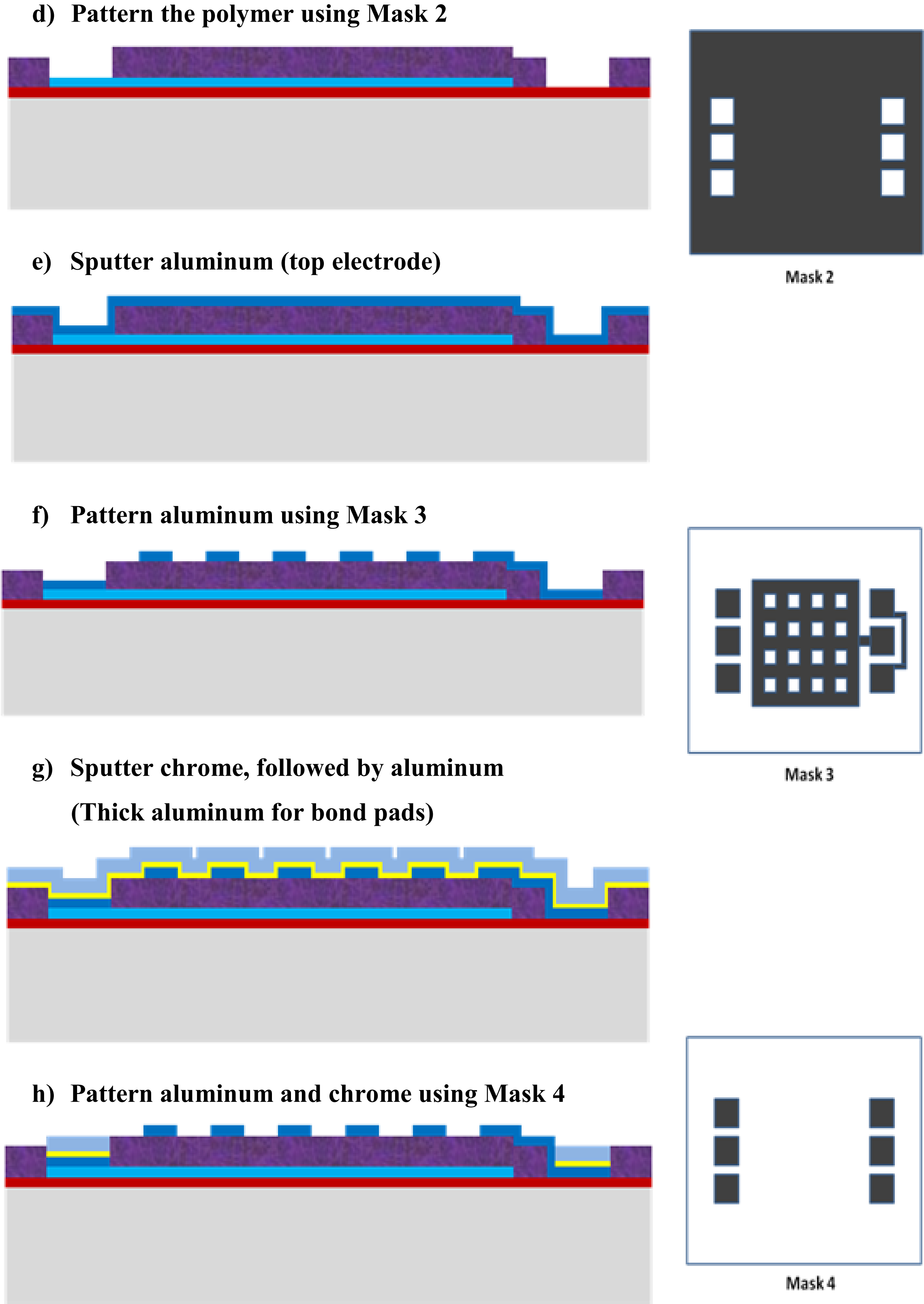

Figure 11-2: Fabrication process flow (horizontal cross-sections shown)

NB: The masks are positive (i.e. the dark regions define where the material being patterned remains). The electrode patterns shown in the mask diagrams are just one example of many different patterns used in this work.

The process flow starts off with a 6-inch <100> silicon wafer that has a 2.5 μm thermal oxide coating on top.

a) 120 nm of aluminum is sputtered. This aluminum will serve as the bottom electrode of the capacitive sensor.

b) Using photolithography (Mask 1), the aluminum is patterned by wet-etching it.

c) 200 nm of the polymer solution (polymer precursor + thinner) is then spin-coated onto the wafer and then cured. The curing procedure immidizes the polymer precursor and drives away all solvents, giving the polymer its physical integrity and defines its ultimate electrical and chemical properties. The curing recipe was optimized to obtain low stress, high quality humidity sensing films.

d) Using photolithography (Mask 2), the polymer is then patterned using reactive-ion-etching (RIE). The patterning is done so as to remove the polymer from the regions of the electrical bond pads.

e) 120 nm of aluminum is sputtered. This aluminum will serve as the top electrode of the capacitive sensor.

f) Using photolithography (Mask 3), the top aluminum is patterned by wet-etching it. As can be noticed form the diagram of Mask 3, the top electrode pattern redefines the bond pads for the bottom electrode. This is done so that the bottom electrode pads don't get etched by the top aluminum etching.

g) A thin layer of chrome is sputtered followed by 300 nm of aluminum. This aluminum serves to increase the thickness of the bond pads. For proper, reliable wire-bonding, it is crucial to have thick metal bond pads. The chrome in this case is used mainly to protect the top electrode aluminum.

h) Using photolithography (Mask 4), the aluminum is patterned by wet-etching it. The etchant does not attack the top electrode aluminum because the chrome provides a protective barrier. Next, the chrome is removed by wet-etching.

NB: It can be noticed from the mask diagrams that each electrode has 3 bond pads. The middle pad is the signal pad and the other two are ground pads. This was done to enable testing using ground-signal-ground (GSG) probes.

This is a 4-mask process that is completely CMOS-compatible. There are no high-temperature steps and all materials and process steps involved are compatible with CMOS processes.

2.5. Design Parameters

The design parameters W (width of top metal) and W_{gap} (width of top electrode opening) are defined in the mask layout. Design-A and B devices with a lot of different variations of W and W_{gap} were included. Also, in addition to having square holes in the top electrode for Design B devices, other variations were included which had circular holes and a honeycomb structure. Devices with both flat bottom electrode and a patterned bottom electrode were included in the mask layout. The goal was to fabricate the different devices and compare their performance.

The other design parameters T_{ue} (top electrode thickness), T_{le} (bottom electrode thickness), and T_P (polymer thickness) cannot be defined in the mask layout. Instead they are set by the deposition recipes used during the fabrication. From the theory and

simulation results discussed in chapter 2, it is evident that using the minimum values for each of these 3 parameters will give the best sensor performance. However, values higher than the minimum were used in this work and this is discussed below.

2.6. Additional Process Flow Steps

2.6.1. Heating the Sensor

Heating the sensors is required after extended periods of use in order to reset the humidity sensing characteristics and cancel any effects that may have been causing a drift in the response. It eliminates dust, dirt, smoke, and other impurities. After extended periods of use in high humidity environments, the polymer may be saturated due to water vapor condensation and returning to a dry state may require some time, during which the sensor is inoperable. If the sensor is heated, it can quickly reset it to its dry state. Heating prevents condensation and increases performance at very high humidity, increasing the operating range of the sensor prior to saturation.

The response time of the sensor is directly proportional to the humidity diffusion constant as shown in equation (5). This diffusion constant is dependent on temperature – it increases with increasing temperature. This means that the sensing device can be heated to boost the diffusion into the polymer layer and hence accelerate the response of the sensor. For these reasons, a serpentine metal heater can be included beneath the capacitive sensing device as shown in Fig. 12-2.

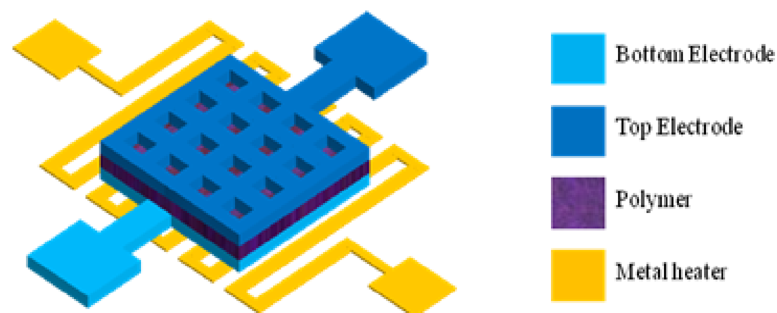

Figure 12-2: Sensing structure on top of a metal heater

The metal heater is fabricated before the sensor and this heater has to be covered with an insulating material to prevent electrical contact between the heater metal and the sensor electrodes. Once this is done, the sensor is then grown on top. Two additional masks will be needed. The additional process flow steps for fabricating a heater at the bottom of the sensor are shown below. These steps come at the start of the process flow shown before (i.e. the additional steps for including the heater are done before the actual sensor device fabrication steps).

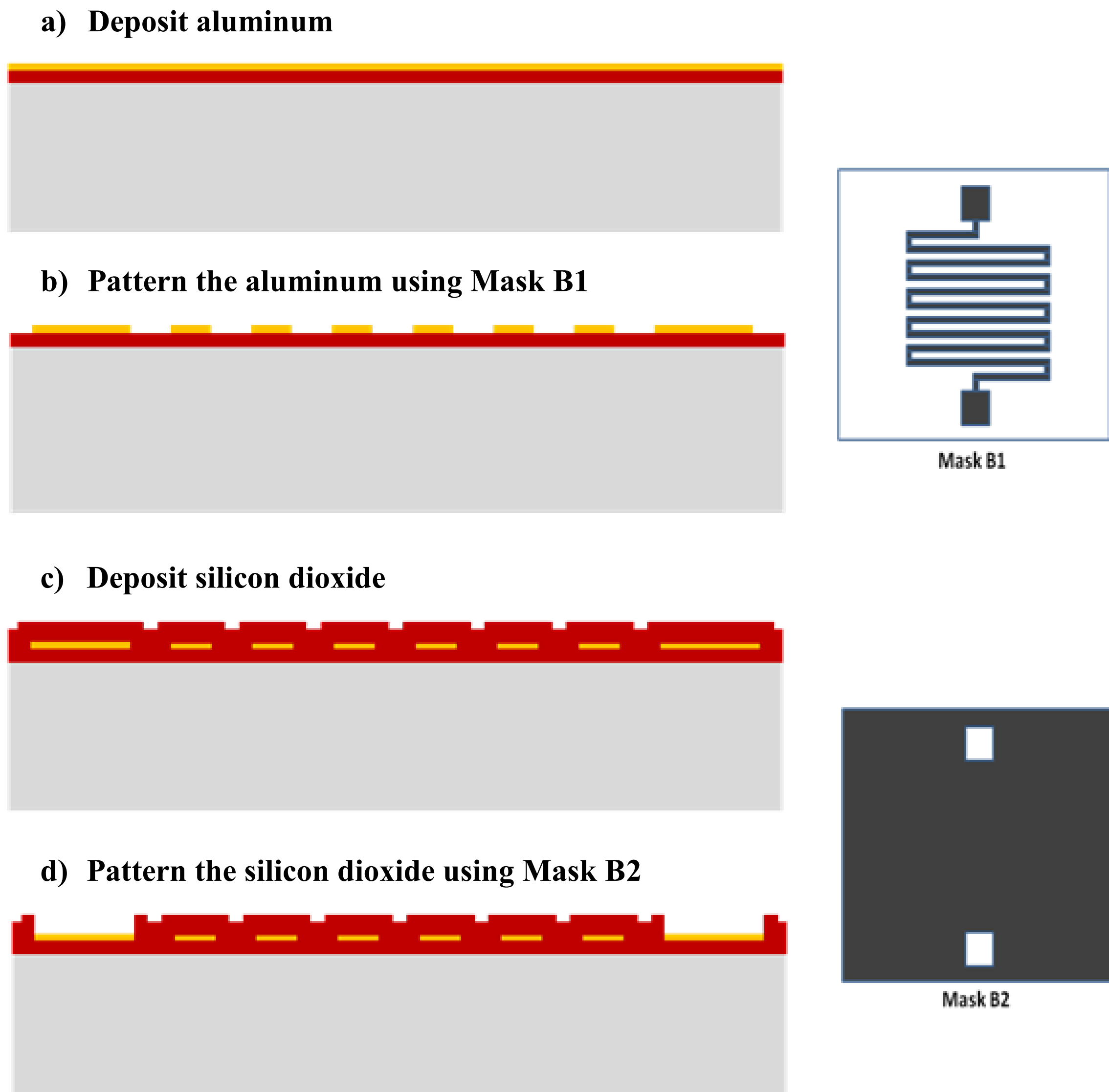

Figure 13-2: Process steps for including a heater layer below the sensor

a) Sputter a thin layer of aluminum. This serves as the heater metal.

b) Using photolithography (Mask B1), the aluminum is patterned by wet-etching it.

c) Using plasma enhanced chemical vapor deposition (PECVD), deposit a layer of silicon dioxide. This insulating layer covers the heater metal in order to electrically isolate it from the sensor that will be fabricated on top. PECVD is used because it is a low-temperature process (≤ 300 ˚C).

d) Using photolithography (Mask B2), pattern the silicon dioxide by reactive-ion-etching (RIE). This patterning involves removing the silicon dioxide from the heater pad regions only in order to expose the heater pads for electrical contact.

2.6.2. Reference Device

The capacitance changes with humidity will be measured using electronic circuitry. This measuring circuit interface usually needs a reference capacitance (independent of humidity) in order to compensate for parameters, that would affect the sensors, other than humidity (e.g. temperature). For this reason, a reference device is designed next to every sensing device as shown in Fig. 14-2. This reference device is exactly the same as the sensing device except for the fact that it is covered with a non-conductive material that is impermeable to moisture. This material will act as a barrier layer to prevent access to moisture and hence the capacitance of the device will be independent of humidity. One suitable material to act as the barrier layer is silicon dioxide (SiO_2). In this work, two other materials were also used tried out as the barrier layer. These are silicon nitride and parylene.

As mentioned earlier, this reference device can also be used for temperature compensation. Temperature variations will always affect the humidity readings. The dielectric constant of the polymer varies with temperature and the sensitivity of capacitive sensors usually increases with ambient temperature. This effect needs to be compensated for.

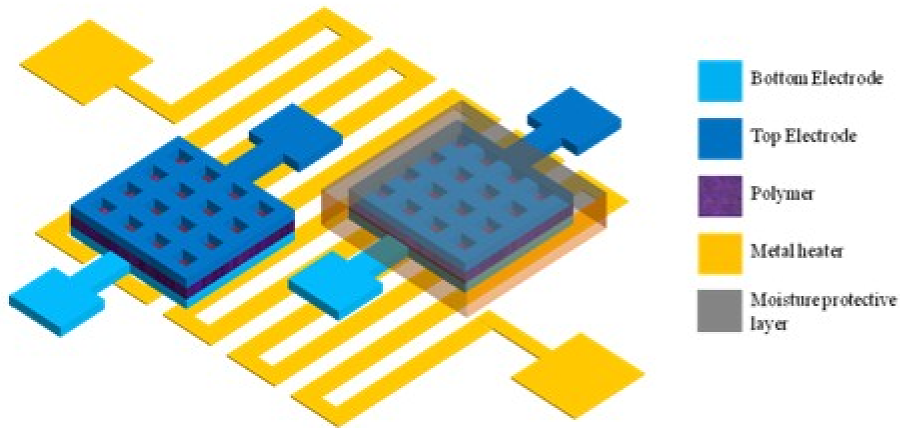

Figure 14-2: Sensing device alongside a reference device

For most humidity sensors, temperature compensation is achieved using integrated temperature sensors in order to adjust the humidity reading with respect to temperature and this is done using circuits. Having a reference device can serve as a temperature sensor. The reference device varies with temperature only, whereas the sensing device varies with both temperature and humidity. This reference can therefore be used to cancel the effect of temperature to a certain degree, depending on the circuit configuration used. Also, a power-expensive way of achieving temperature compensation can use a closed feed-back loop to control the current to the heater (beneath the sensing device), such that the temperature of the device is fixed at a certain value.

For fabricating the sensor device along with its reference, two identical sensors are fabricated next to each other and one is covered with a moisture-impermeable layer. One additional mask is needed for this. The additional process steps required for creating the reference device are shown below.

a) Deposit the moisture impermeable protective layer

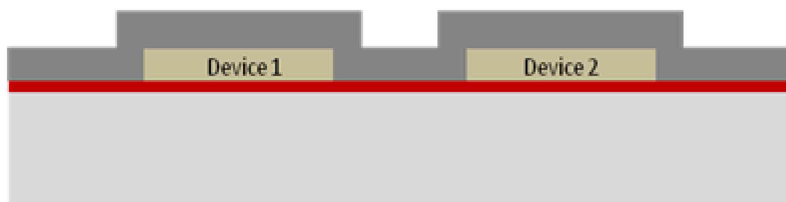

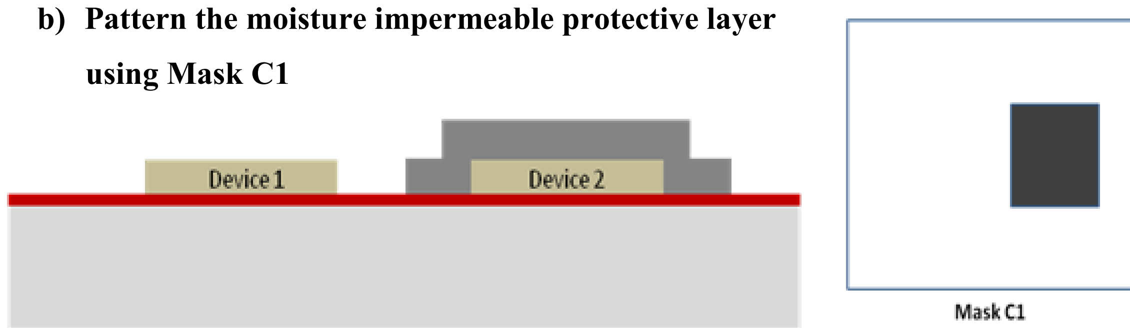

Figure 15-2: Additional process steps for creating reference devices (horizontal cross-sections shown)

a) After two identical sensors have been fabricated next to each other using the original process flow, the moisture impermeable layer is deposited.

b) Using photolithography (Mask C1), the protective layer is patterned by reactive-ion-etching (RIE).

The protective layers used in this work were silicon dioxide, silicon nitride, and parylene. Parylene CVD is a low-temperature process (≤ 300 ˚C). Plasma enhanced chemical vapor deposition (PECVD) was used to deposit silicon oxide and nitride. This is because PECVD is a low-temperature process (≤ 300 ˚C). Keeping the temperature low keeps the entire process CMOS compatible and also protects the other layers in the process. For example, if thermal deposition of silicon oxide is used instead, the temperatures for this process can get up to 1000 ˚C. Not only does this make the entire process CMOS incompatible, but other layers such as the aluminum electrodes will be melted or degraded.

2.7. MATLAB Simulation Model

2.7.1. Theory of Capacitive Humidity Sensing

Sensing humidity using capacitive sensor structures is based on the model shown below in Fig. 16-2. Water vapor molecules are adsorbed onto the surface of the polymer,

followed by diffusion of the vapor molecules into the bulk of the polymer, inducing a change in the permittivity of the polymer.

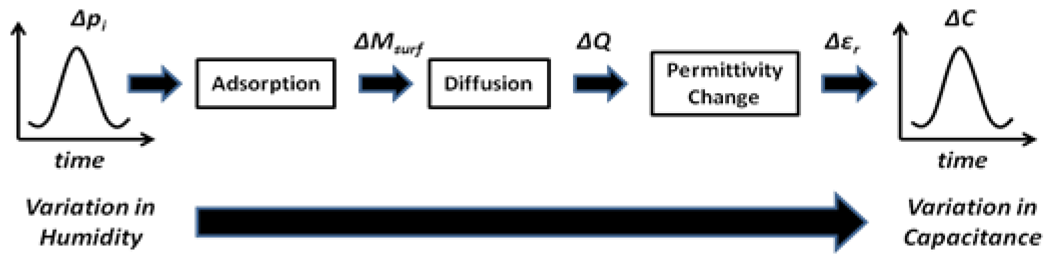

Figure 16-2: Steps involved in capacitive humidity sensing

Variation in ambient humidity translates to a change in the amount of moisture in air, which in turn results in the variation of the partial vapor pressure (Δp_i). This change in vapor pressure leads to a variation in the polymer surface concentration of adsorbed water vapor molecules (ΔM_{surf}). The surface molecules then diffuse into the polymer, causing a change in the total amount of water (ΔQ) in the polymer. The shift in the total amount of water sorbed induces a change in the permittivity of the polymer ($\Delta \varepsilon_r$), which translates into a change in capacitance (ΔC) of the sensing structure.

Surface Concentration

Adsorption of the penetrant (water vapor) molecules onto the surface of the polymer changes the surface concentration of these molecules. This phenomenon can be viewed as water vapor dissolving in the polymer. If a quasistatic equilibrium state is assumed between the polymer surface and the water vapor, then the sorption mechanism can be modeled using Henry's law. This law states that the concentration of the solute (water vapor) sorbed or dissolved onto the polymer is directly proportional to the partial pressure of the vapor above the polymer and can be expressed mathematically as follows:

$$M_{surf} = k_D p_i \quad \ldots\ldots\ldots(9)$$

In equation (9), M_{surf} is the penetrant concentration on the polymer surface, p_i is the partial vapor pressure above the polymer, and k_D is the Henry's law dissolution constant. In glassy polymers such as the polymer used in this work, Henry's law dominates the sorption mechanism. However, glassy polymers usually have microvoids or holes throughout and these microvoids act to immobilize some of the penetrant molecules.

While Henry’s law models the ordinary dissolution, the sorption in microvoids or holes can be described by a Langmuir isotherm. Hence, sorption can be modeled as two concurrent mechanisms – normal dissolution and hole-filling. This dual mode sorption can be expressed mathematically as:

$$M_{surf} = k_D p_i + \frac{C'_H b p_i}{1 + b p_i} \quad \ldots \ldots \ldots (10)$$

In equation (10),   is the hole saturation constant and *b* is the hole affinity constant. If the polymer film is considered thick enough, then the adsorption kinetics can be neglected compared to the diffusion kinetics and the surface can be assumed to be in quasistatic equilibrium with the water vapor. In such a case, the dual mode sorption is a valid model for the surface concentration.

Concentration in the Film

The penetrant molecules on the polymer surface diffuse into the polymer and this induces a change in the concentration of the penetrant within the polymer film over time. The change in concentration over time can be expressed using Fick’s diffusion law:

$$\frac{\partial \Delta M(x,y,z,t)}{\partial t} = D_x \frac{\partial^2 M}{\partial x^2} + D_y \frac{\partial^2 M}{\partial y^2} + D_z \frac{\partial^2 M}{\partial z^2} \quad \ldots \ldots \ldots (11)$$

In equation (11), *D* is diffusion constant. This equation expresses Fick’s law over all three dimensions (x, y, and z). Diffusion of the moisture into the polymer occurs both vertically from the surface of the polymer into the bulk of the polymer and laterally inside the polymer. The diffusion constant is defined by the polymer and if dual-mode sorption (Henry’s law and Langmuir isotherm) is considered, an effective diffusion constant can be considered as expressed in equation (12):

$$D_{eff} = \frac{D}{1 + \frac{C'_H b}{k_D (1 + b p_i)^2}} \quad \ldots \ldots \ldots (12)$$

Permittivity of the Polymer

The diffusion of the vapor into the polymer changes the overall amount of water (*ΔQ*) in the polymer film with time. This can be obtained by integrating over the x, y, and z directions. The total amount of water determines the number of dipoles per unit volume (*N*) of the polymer and this sets the overall permittivity of the polymer. This permittivity is related to *N* by the following formula:

$$\frac{\Delta N\alpha}{3\varepsilon_o} = \frac{\varepsilon_{r(RH)} - 1}{\varepsilon_{r(RH)} + 2} - \frac{\varepsilon_{r(0)} - 1}{\varepsilon_{r(0)} + 2} \quad \dots\dots\dots (13)$$

In equation (13), $\varepsilon_{r(0)}$ is the dry relative permittivity (no water sorption) and $\varepsilon_{r(RH)}$ is the relative permittivity after water sorption ($\varepsilon_{r(0)}+\Delta\varepsilon_r$).

Capacitance Change

The change in permittivity due to sorption changes the capacitance of the sensing structure and this is given by:

$$\Delta C = \frac{\Delta\varepsilon_r \varepsilon_0 A}{d} \quad \dots\dots\dots (14)$$

In equation (14), *A* is the area of overlap between the two electrodes and *d* is the distance between them.

The theory behind capacitive humidity sensing (i.e. how a change in humidity results in a change in capacitance of the sensing structure) has been described above. The simulation model is based on this theory.

2.7.2. Simulation Model

The simulation model measures the dynamic response of the sensor when subjected to ambient humidity changes. The simulation model follows the sequence shown in Fig. 16-2. When the ambient humidity changes, the corresponding change in the polymer surface concentration of adsorbed vapor molecules (ΔM_{surf}) is calculated. ΔM_{surf} is considered to be the input to a system whose response is defined by Fick's diffusion law (Equation 11).

The output is computed by convoluting the input with the impulse response of the system as done for conventional LTI (linear time invariant) systems. This output gives the total amount of water in the polymer film as a function of time, which is then used to compute the corresponding change in permittivity of the polymer (Equation 13). The permittivity is then used to estimate the corresponding capacitance of the sensor.

The simulation model operates by convoluting the input to the system (humidity variations) with the impulse response of the system, to give the output (sensor capacitance variation). This is illustrated in Fig. 17-2.

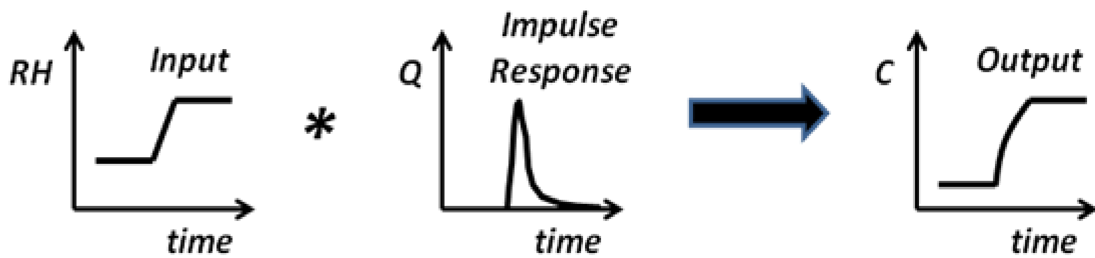

Figure 17-2: Simulation model

Impulse Response

The impulse response of the system is the solution of Fick's diffusion law subject to an input impulse. In other words, the impulse response is the solution of the partial differential equation shown below (Equation 15) for boundary conditions that corresponds to an impulse input.

$$\frac{\partial \Delta M(x,y,z,t)}{\partial t} = D_x \frac{\partial^2 M}{\partial x^2} + D_y \frac{\partial^2 M}{\partial y^2} + D_z \frac{\partial^2 M}{\partial z^2} \quad \dots\dots\dots (15)$$

Equation 7 is a 3-dimensional partial differential equation (PDE). This represents the diffusion of vapor molecules in all three dimensions (x, y, and z directions). This 3-dimensional case can be simplified by treating the 3-dimensional diffusion phenomena as separate unidirectional diffusion cases. For diffusion in one direction only, Fick's diffusion law can be written as:

$$\frac{\partial \Delta M(y,t)}{\partial t} = D_y \frac{\partial^2 M}{\partial y^2} \quad \dots\dots\dots (16)$$

This simplifies computation in that the system is now described by a 1-dimensional PDE instead of a 3-dimensional PDE. The impulse response of the overall diffusion process will be the sum of the impulse responses of the individual 1-dimensional cases. The impulse response of Equation 8 can be calculated by first finding the step response and then taking the derivative of the step response to get the impulse response. By studying the mathematics of diffusion [1], the step response of the PDE in Equation (16) can be computed to be:

$$M_s = M_o - \frac{4M_o}{\pi}\sum_{n=0}^{\infty}\frac{(-1)^n}{2n+1} exp\left[\frac{-D(2n+1)^2\pi^2 t}{4L^2}\right]\cos\left[\frac{(2n+1)\pi y}{2L}\right] \quad \dots\dots\dots(17)$$

In Equation 17, M_S is the step response, M_o is the initial surface vapor concentration, D is the rate of diffusion in the polymer, L is the thickness of the polymer, y is the distance from the surface of the polymer into the bulk of the polymer, and t is time.

The impulse response can be obtained by taking the time derivative of the step response. To compute the impulse response for the total amount of water vapor in the polymer film, M_I is integrated over the thickness of the polymer as shown in Equation 18.

$$Q_I = \int_0^L M_I\, dy = \frac{2DM_o}{L}\sum_{n=0}^{\infty} exp\left[\frac{-D(2n+1)^2\pi^2 t}{4L^2}\right] \quad \dots\dots\dots(18)$$

Equation 18 shows the impulse response for diffusion in the y-direction (vertical direction). The impulse response for diffusion in the other directions will be similar, except that the parameter, L, will represent a thickness in a different direction. The overall impulse response of the system is the sum of the individual 1-dimensional impulse responses.

2.8. References

[1] “Mathematics of Diffusion”, J. Crank, 2nd edition, 1979

[2] A. Tetelin, V. Pouget, J. L. Lachaud, and C. Pellet, “Dynamic Behavior of a Chemical Sensor for Real-Time Measurement of Humidity Variations in Human Breath”, *Instrumentation and Measurement Technology Conference*, May 2003.

[3] A. Tetelin, C. Pellet, C. Laville, and G. N’Kaoua, “Fast response humidity sensors for a medical microsystem”, *Sensors and Actuators B*, pp. 211-218, 2003.

[4] D. D. Denton, J. B. Camou, and S. D. Senturia, “Effects of the moisture uptake on the dielectric permittivity of polyimide films”, *Solid-State Sensors and Actuators*, June 1985.

3. Fabrication/Testing / CMOS Integration

3.1. Microfabrication

Recipes to deposit the required thickness of each layer in the process flow with high quality were developed and optimized in the microfabrication lab. The complete detailed process flow, along with all the recipes, techniques, and materials used are described in separate documents.

3.1.1. Packaging

Once the devices were fabricated, they were diced manually at the McGill Nanotools Assembly Room and packaged in 28-pin Leadless Chip Carrier (LCC) packages. Fig. 1-3 below shows a picture of a packaged die containing multiple sensor devices.

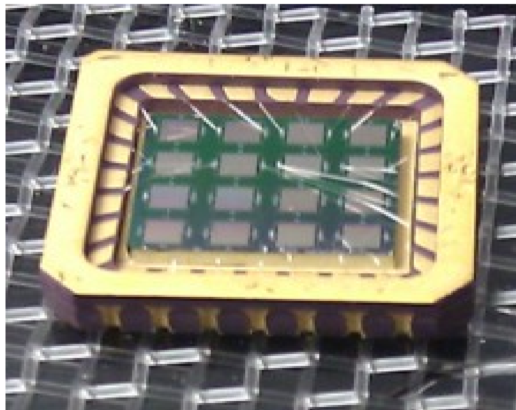

Figure 1-3: Packaged die with sensors

3.2. Testing Procedures and Results

3.2.1. Deliquescent Salts Testing

Once the first batch of devices was successfully fabricated, they were tested for basic functionality simply to make sure that the devices were operational and to confirm that

the fabrication was done adequately. This was done by verifying that the sensor devices had the expected capacitance values and that their capacitances varied with humidity. An LCR meter was used to measure the capacitance (at 10 kHz and 1V input). Initially, there was no humidity chamber available, and hence deliquescent salts were used to provide varying humidity levels.

Deliquescent salts have a strong affinity for moisture and absorb large amounts of water vapor from the surrounding air. If a saturated solution of the salt is enclosed in an air-tight environment, the humidity of the surrounding air is set to a very specific value. There are a variety of deliquescent salts, each providing a different humidity level. These salts provide a very reliable and accurate humidity setting and are used commercially for humidity sensor calibration.

Four different salts were used to generate four different humidity levels. The sensor to be tested was enclosed in an in-house custom-made air-tight chamber with each salt and its capacitance was measured. The test setup is shown in Fig. 2-3. The sensor package was placed on the test PCB. The PCB was then mechanically sealed to a chamber containing the saturated deliquescent salt solution. Electrical connections were made to the other face of the PCB using SMA connectors.

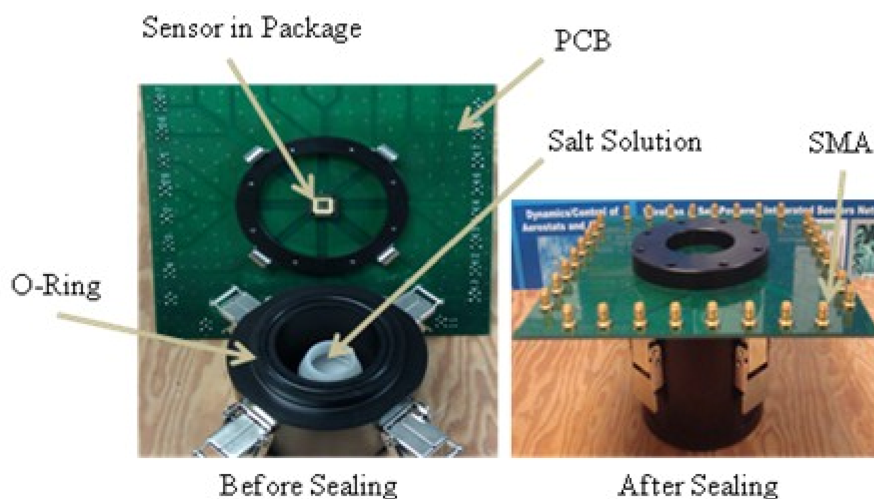

Figure 2-3: Deliquescent Salts Testing Setup

The seal was achieved using a lubricated O-ring and 4 clamps, providing a very air-tight setup. The clamps can easily be released for changing the die or the salt solution, enabling the testing of as many dies as required, using multiple salt solutions. The saturated salt solutions were prepared by mixing the salt with de-ionized water in a very specific ratio. This ratio was obtained from the user manual of the Vaisala relative humidity sensor calibration kit [1]. The salts used and their corresponding humidity levels, as well as the mixing amounts of salt and de-ionized water are shown in Table 1-3.

After sealing the PCB to the chamber, the solution was allowed to stand for 24 hours before taking measurements. This is to ensure that the humidity inside the chamber stabilizes to the desired value.

Salt	Amount of Salt/De-ionized Water	%RH at Room Temperature
Lithium Chloride ($LiCl_2$)	15 g / 12 ml	11
Magnesium Chloride ($MgCl_2$)	30 g / 3 ml	33
Sodium Chloride (NaCl)	20 g / 10 ml	75
Potassium Sulphate (K_2SO_4)	30g / 10 ml	97

Table 1-3: Deliquescent salt/de-ionized water ratio and corresponding relative humidity

Testing all the devices against the salts showed that the sensors had the expected capacitance values and their capacitance was different for every salt (humidity). All devices showed a very linear capacitance-humidity relationship. An example of a plot obtained is shown below.

As can be seen from the plot, the response is very linear (**R^2 = 0.9996**), and the sensitivity is around **24.56%**. This device has a sensing area of 0.25 mm x 0.25 mm, with a flat bottom electrode and a top electrode patterned with square holes (W = 25 µm, W_{gap} = 5 µm). The simulated sensitivity is 27.45 %. The measured sensitivity is expected to be lower due to the parasitic capacitances added from the die, package, and test PCB. Also, as mentioned earlier, the simulations were based on certain theoretical values such as the

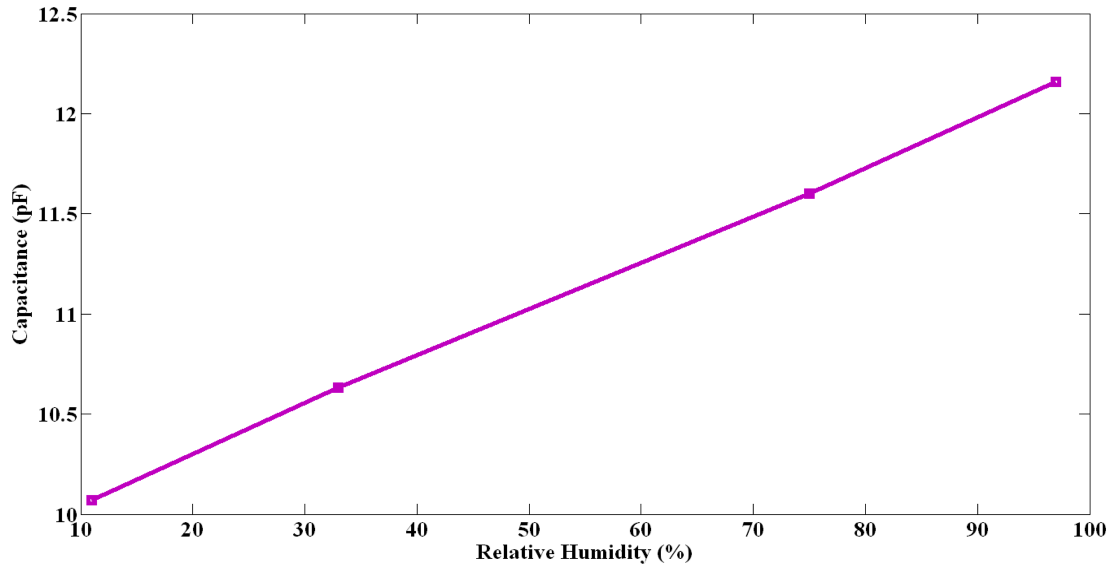

Figure 3-3: Sensor capacitance against relative humidity obtained using deliquescent salts testing

total moisture absorption of the polymer and the calculated values of the dielectric constant of the polymer at 0 and 100 %RH. These values may be different for the actual devices. Finally, for practical measurements, the variation of the dielectric constant of the polymer with humidity depends on the LCR meter test frequency, which is not the case in simulations.

The deliquescent salt testing was only done as a preliminary test to check if the initial fabricated devices were functional. Only a few devices were tested using this method when there was no humidity chamber available. All further tests were done using a humidity/temperature climate chamber.

3.2.2. Sensitivity / Hysteresis Testing

A humidity/temperature chamber was used for sensitivity and hysteresis tests. The chamber was maintained at a constant temperature (25 deg C) and the humidity was cycled up and down. Five different humidity settings were used (from 30 %RH to 90 %RH) and the chamber was allowed to stabilize for 20 minutes at each setting. The minimum humidity level the chamber could reach at room temperature was 30 %RH. The chamber has an accuracy of ±2 %RH and it fluctuates about the set humidity value by up to 6 %RH. A reference humidity meter from Vaisala was used as a reference to record the

relative humidity values. This meter has an accuracy of about ±2 %RH. An LCR meter was used to measure the capacitance at 10 kHz and 1V input. Each test die had several sensor devices on it. A different test PCB was designed which had multiplexers and a microcontroller to enable switching between the various devices on the die through a computer from outside the chamber. The results obtained for all the various devices are shown and discussed next.

Fig. 4-3 below shows the sensitivity and hysteresis plot obtained for one of the devices. The device is Design-A type with a flat bottom electrode and $W = W_{gap} = 5$ µm. The measured sensitivity is around **22.51%** and the maximum hysteresis at 60 %RH is around **3.52 %RH**.

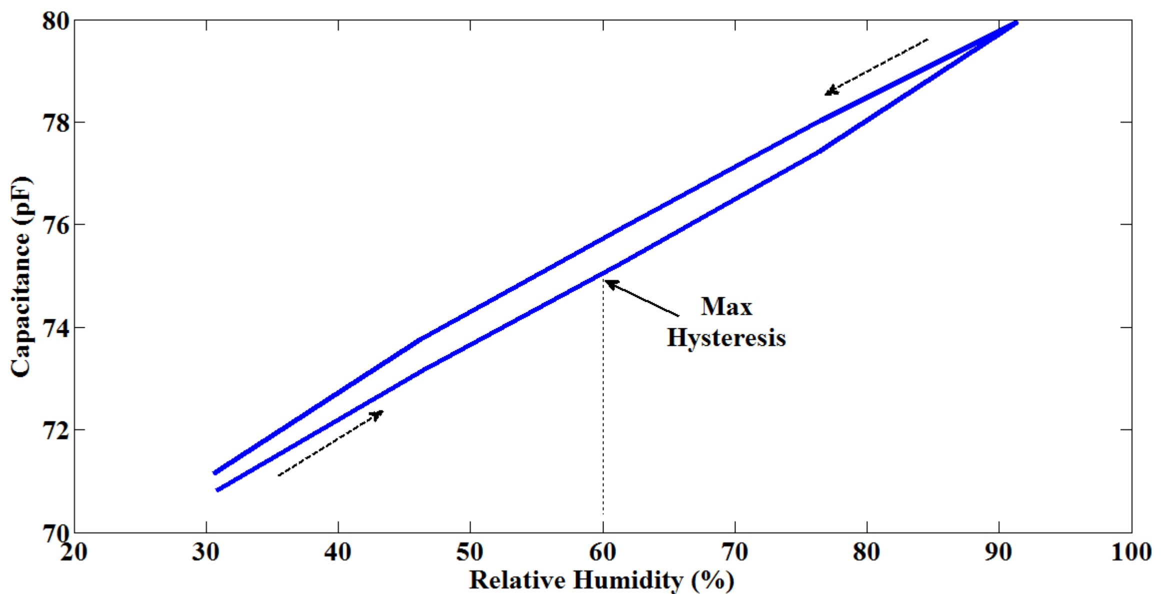

Figure 4-3: Measured sensor capacitance against relative humidity

The sensitivity and hysteresis of a whole variety of other devices were tested. These included both Design-A type and Design-B type devices with varying W and W_{gap}, other variations which had circular and honeycomb structure holes on the top electrode, and devices which had both flat and patterned bottom electrodes. In terms of sensitivity, it was impossible to compare the various devices since there was no particular trend. This is expected because the sensitivity differences are expected to be very small amongst the various devices as noticed from simulations. For example, the sensitivity difference

between having $W = 2$ µm and $W = 25$ µm is about 7%, the sensitivity difference between having a flat bottom electrode and a patterned bottom electrode is only about 2.5%, while the sensitivity difference between Design-A type and Design-B type is also about 2.5%. These small differences are very hard to notice from practical measurements. It was noticed that exactly identical devices showed difference in sensitivities as large as 6%. This combined with parasitic capacitances, measurement errors, different capacitance values for the various devices, and inaccuracies of the humidity chamber and reference humidity meter, all serve to mask the small sensitivity differences amongst the various designs, and hence cannot be noticed from practical measurements. One possible solution could be to fabricate and test a large number of identical devices of each design type and compare the mean sensitivities. This was not done in this work. Only two identical devices of each design type were fabricated and tested, which is not sufficient to notice any trend amongst different designs.

The sensitivities of all devices tested ranged from **21% to 24.5%** and they all showed very high linearity (**$R^2 > 0.99$**).

The hysteresis was also measured for each device. Theoretically, the hysteresis is a property of the polymer and should not depend on device geometry. However, there was one trend noticed from the hysteresis measurements. The devices that had a patterned bottom electrode showed a higher hysteresis than the devices which had a flat bottom electrode. All devices exhibited maximum hysteresis around 60 %RH. The maximum hysteresis values of several devices with flat and patterned bottom electrodes are shown in Fig. 5-3 below.

The possible reasoning behind this observed result could be that the polymer in the small pocket regions formed by the openings in the bottom electrode boosts the clustering of vapor molecules and hence, enhances hysteresis. With a flat bottom electrode, these pockets are not present and as a result, hysteresis is lower.

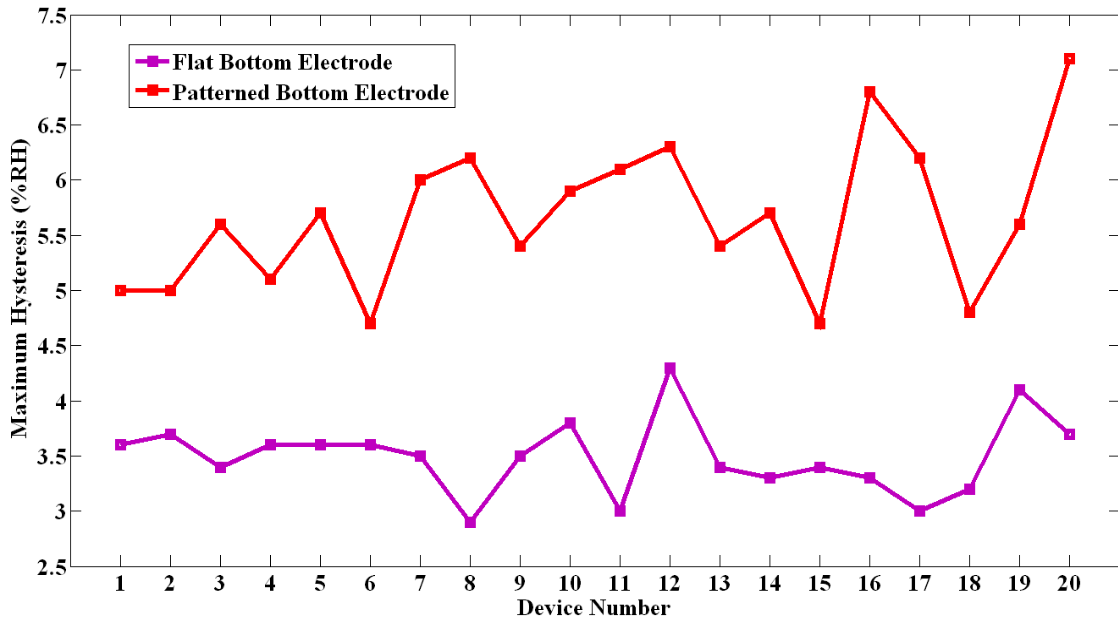

Figure 5-3: Maximum hysteresis of several devices with both flat and patterned bottom electrodes

3.2.3. Response Time Testing

A crucial performance specification for relative humidity sensors is the response time. This is defined as the time it takes for the sensor to respond to an abrupt humidity change (a humidity step). Testing for response time can be a very difficult task since a setup has to be designed that allows the sensor to be exposed to a relative humidity step. In other words, the sensor has to be stabilized in one environment with a particular humidity level and introduced into another environment with a higher stable humidity level. This switch has to be immediate like a step function and the corresponding instantaneous capacitance change of the sensor has to be measured. The setup which was in-house custom devised to achieve this is shown in Fig. 6-3.

A thin latex membrane is tightly stretched (as indicated by the dashed arrows) over the circular surface of the stand. The PCB, with the sensor on its underside, is pushed into the circular opening on the stand. The opposite side of the PCB has all the electrical connectors providing connections to the sensor devices in the package. The protruding ring (with the o-ring) from the underside of the PCB pushes the membrane through and perfectly fits into the circular opening on the stand surface, with the membrane

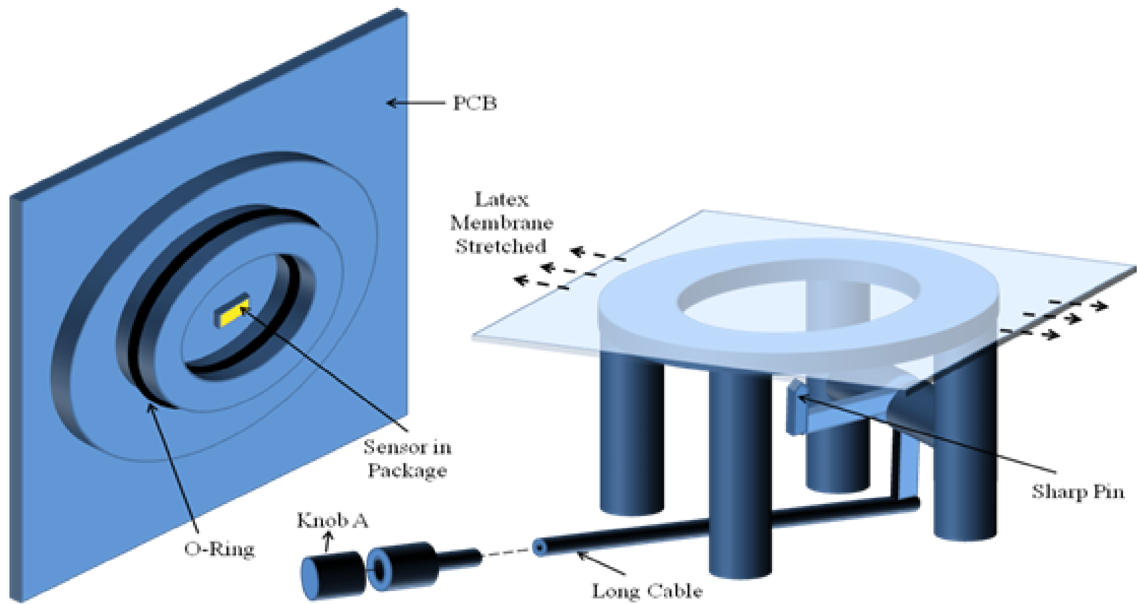

Figure 6-3: Response Time Test Setup

conforming around it. The o-ring, when lubricated, serves to form a perfect seal. As a result, the sensor is sealed in a small pocket formed between the PCB and the membrane. This sealing is done at room humidity and temperature (~ 45 %RH and 25 °C). The whole setup is then placed inside a humidity/temperature chamber. The long cable comes as well as the electrical connecting cables, comes out through a small opening in the chamber so that knob A is accessible outside the chamber. This small hole in the chamber is closed with a silicone rubber. The chamber is closed and allowed to stabilize to 70 %RH and 25 °C.

While the chamber is at 70 %RH, the sensor is still sealed in the small pocket between the membrane and the PCB at room humidity. Once the chamber has stabilized at 70 %RH, knob A is pulled from outside the chamber, which causes the sharp pin to move upwards. This swiftly snaps the latex membrane, exposing the sensor immediately to the chamber environment. The sensor is thus exposed to a humidity step – an immediate change from room humidity environment to the 70% chamber humidity. The corresponding instantaneous capacitance change of the sensor is monitored using an LCR meter. The LCR meter is used in remote mode and controlled using a MATLAB script which tracks the capacitance change. The results obtained are discussed next.

Fig. 7-3 below shows the response of a Design-A type and Design-B type device, both with a top metal width, *W* of 5 µm. The simulation result is also shown in the form of the dashed curve.

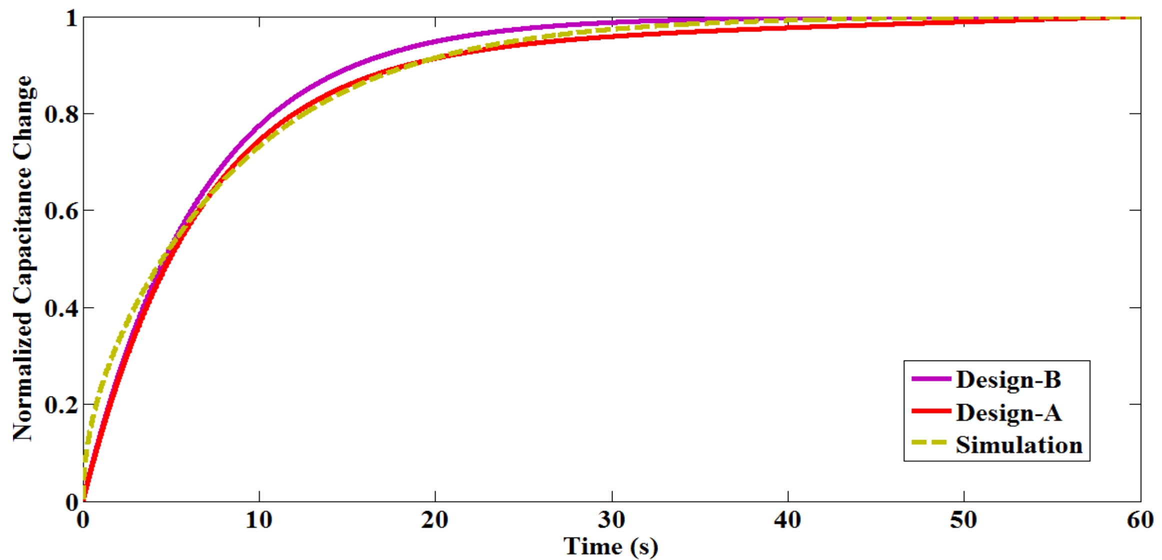

Figure 7-3: Response time plot of to devices along with the simulation result

As can be seen from Fig. 7-3, the response of the Design-A type device is slightly faster. The table below shows the calculated response time values of these devices, along with the values of other devices with different top metal widths. The response time is calculated by first curve fitting the raw data from the LCR meter and calculating the time constant, which is the time it takes for 63% of the capacitance to occur.

***W* (µm)**	**Response Time (s)**		
	Design-B (Fingers)	**Design-A (Square Holes)**	**Simulation**
2	1.5	2.2	1.1
3	2.5	3.1	2.6
4	4.0	4.6	4.6
5	6.7	7.3	7.2
10	27.5	30.8	28.9
15	50	69.5	64.9

Table 2-3: Measured and simulated response time values for Design-A and Design-B type devices of varying *W*

Design-B type devices with the smallest top metal width ($W = 2\mu m$) showed the fastest response with a response time of **1.5 s**. The table clearly shows that sensors that have square holes in the top electrode (Design-A) have a slightly slower response than the sensors with fingers as the top electrode (Design-B). As can be recalled from chapter 2, the simulation model shows identical response for Design-A and Design-B type devices. However, the measured results show that there is a difference between the responses of the two types of devices. This could be due to the fact that the diffusion constant in reality is a function of the moisture concentration profile. The entire simulation model is based on Fick's Diffusion Law, which was solved assuming a constant diffusion constant throughout the response duration. In reality, this constant is a function of the moisture concentration profile, which is a function of distance and time. In Design-A type devices, the moisture diffuses into 4 different directions (4 sides of each square hole). As a result, the moisture concentration in each diffusion direction is lower than in Design-B where diffusion occurs in only two directions. This results in a lower total effective diffusion constant in Design-A devices, giving them the slower response. Also, as moisture diffuses deeper into the polymer, the concentration reduces, which serves to reduce the effective diffusion constant in reality. This is perhaps why the measured results show a slower response than the simulation for larger W and also probably why the difference between Design-A and Design-B devices become larger for a higher W.

From the response time results, it was seen that the pattern of the top metal influences the response time. Some other patterns (circular holes and a honeycomb structure) were fabricated and tested to see how the response time is influenced. The plot below (Fig. 8-3) shows the response of the 4 different patterns for $W = 10\ \mu m$. A large top metal width (W) was used for comparison in order to be able to clearly differentiate the response. For faster devices, the response time values are small and the differences between different designs may be masked by measurement and calculation errors.

As can be seen from the plot, the best response is obtained when the sensors have fingers as the top electrode pattern (**27.5 s**). The square-hole pattern offers slightly slower

response (**30.8 s**). The honeycomb structure is even slower (**38 s**) and the sensors with circular holes exhibit the slowest response (**54 s**).

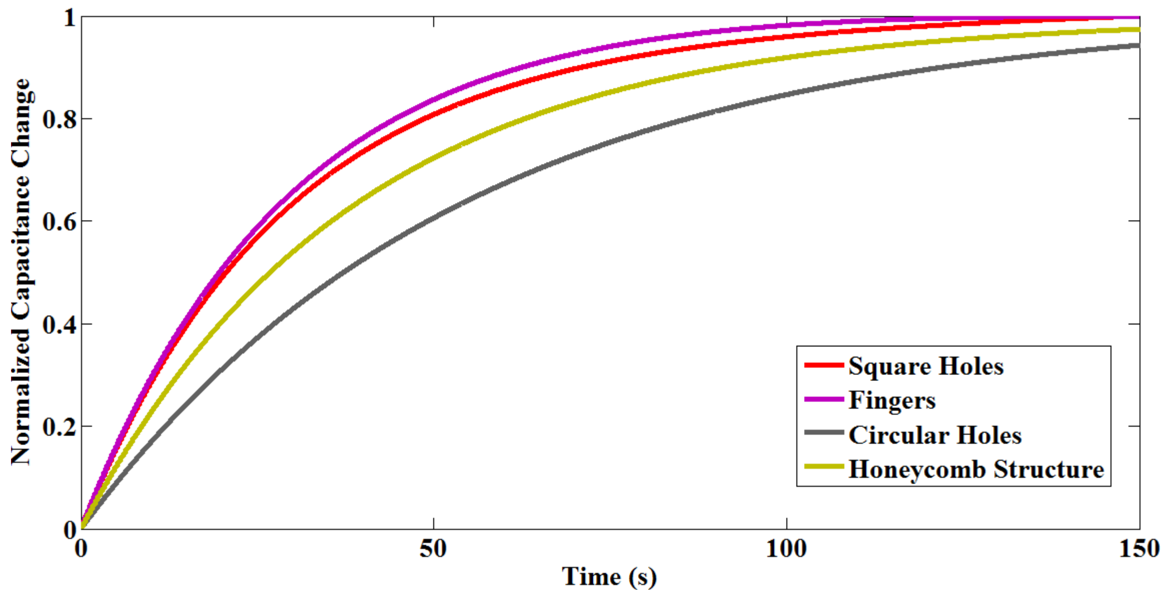

Figure 8-3: Comparison of the responses of sensors with different top electrode patterns

Recovery Time

The recovery time of the sensors is of the same order and proportional to the response time. The plot below (Fig. 9-3) shows the recovery time of fast and slow devices for both Design-A and Design-B and Table 3-3 gives the exact values. Similar to the response time, the recovery times for Design-B devices are faster than Design-A and this difference becomes more prominent for larger W. The recovery times are slightly slower than the response times or even faster in the case of Design-B with $W = 15$ μm.

The rate of diffusion of moisture from the ambient air into the pores of the polymer is usually faster than the rate of diffusion out of the pores into the surrounding air. Most of the previous work reported in literature show recovery times that are much slower than the response times for polymer based capacitive humidity sensors. However, the designs in this work show recovery times that are only slightly larger or even smaller in some cases. This shows the excellent humidity sensing quality of the polymer film used in this work, with no imperfections, and very uniform pore sizes and distribution.

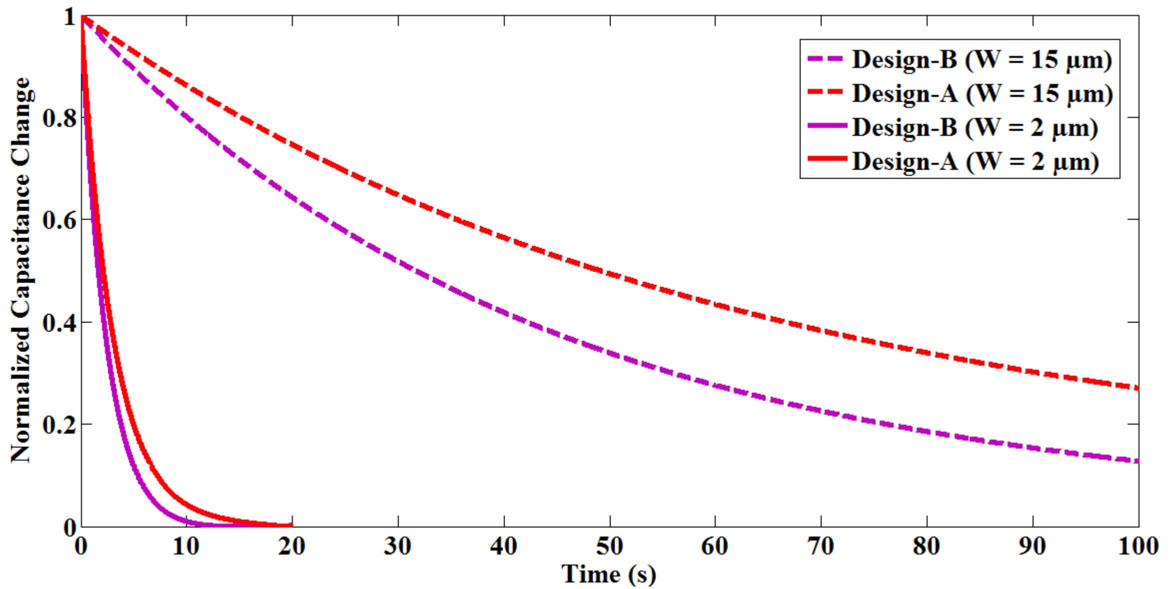

Figure 9-3: Plot showing the recovery times of fast and slow devices for both Design-A and Design-B type devices

	Design-A		Design-B	
	$W = 2$ μm	$W = 15$ μm	$W = 2$ μm	$W = 15$ μm
Recovery Time (s)	**3.0**	**72**	**2.3**	**46**
Response Time (s)	2.2	69.5	1.5	50

Table 3-3: Recovery and response time values of fast and slow devices for both Design-A and Design-B type

3.2.4. Stability Testing

Deliquescent salts were used for this test. The sensors were sealed in a chamber (Fig. 2-3) with a saturated solution of sodium chloride. This provides a very accurate relative humidity level of 75%. After allowing 24 hours for the chamber environment to stabilize, the capacitances of the sensors were monitored with time. The stability of the devices was tested both over a short period (3 hours) and a long period (120 hours).

Stability - 3 Hours

Over three hours, the average value of the capacitance of each device remained perfectly stable with no drift.

Stability – 120 Hours

When exposed to high humidity over an extended time period, the sensors undergo a reversible drift - the sensor capacitance slowly increases with time. This phenomenon is known as 'sensor creep'. The average creep over 120 hours at 75 %RH was about **0.9%** capacitance variation for both Design-A and Design-B type devices. This creep is a reversible process – it resets once the sensor is removed from the high humidity exposure.

3.2.5. Long Term Drift

As the sensor ages, it will experience some level of drift over the years, which is a random process. It is not practical to measure the performance of the sensor over multiple years. In this work, the aging of the sensors was achieved by exposing the sensors to a high temperature over certain duration. The aging at a higher temperature corresponds to a much longer aging period at a lower temperature and this can be calculated by using the Arrhenius equation which relates reaction rate to temperature. This equation is shown below.

$$k = Aexp\left(\frac{E_a}{RT}\right) \quad \dots\dots\dots(19)$$

A is a constant, E_a is the activation energy, R is the Boltzmann constant, T is the temperature in Kelvin and k is the reaction rate. This equation can be modified to express the relation between reactions at two different temperatures. This relation is shown below.

$$t_L = t_H \exp\left(\frac{E_a}{R}\left(\frac{1}{T_H} - \frac{1}{T_L}\right)\right)^{-1} \quad \dots\dots\dots(20)$$

T_H and T_L represent the high and low temperatures (in Kelvin) respectively, while t_H and t_L correspond to the aging duration (in hours) at the high and low temperatures respectively. If the sensor is aged at a higher temperature for a given time, the corresponding aging duration at a lower temperature can be calculated using this equation.

The sensors were aged at 125 °C for 50 hours. Using equation (20) and 0.69 eV as the activation energy for hydrolytic degradation of the polymer, this corresponds to an aging of about 5 years at 25 °C.

Once the high temperature exposure is completed, an offset was noticed in the sensor capacitance values. This is due to the baking of the sensors which results in all moisture being driven away. This offset can be corrected by rehydrating the sensors.

It should be noted that it is quite difficult to determine the exact rehydration process. If done too long, the sensors will be over hydrated and the offset due to baking will be over compensated for. If done too short, the sensors will not be rehydrated enough and the offset will not be nullified completely. In this work, the sensors were rehydrated by exposing them to 75 %RH at 25 °C for about 24h. This was done by sealing the sensors with a saturated solution of Sodium Chloride, which provides an accurate relative humidity level of 75%. The sensor capacitance values were then measured and the differences from the initial measurements before the high temperature exposure were calculated. This difference divided by the aging duration gives the long term drift of the sensors.

Average long term drift of devices in the 2-8 pF range ≈ **0.1 %RH/year**

Average long term drift of devices in the 40-90 pF range ≈ **0.9 %RH/year**

Average long term drift of devices in the 150-180 pF range ≈ **1.7 %RH/year**

It was noticed that the long term drift was higher for devices with larger capacitances. This is because more of the aged polymer is part of the active capacitance of the device. Larger capacitance devices are basically devices that have a larger electrode overlap area. This implies that more of the aged polymer is part of the active capacitance of the device, and hence there is a greater effect of aging on the sensor. Design-B type devices (devices with fingers) generally have lower electrode overlap area than devices with holes, and

therefore show less long term drift. It can be concluded that minimizing the overall sensor size and the electrode overlap area (through electrode patterning) will minimize the long term drift.

3.2.6. Reference Device Testing

As mentioned earlier, three different materials were tried as the moisture shielding layer for the reference devices, namely silicon dioxide, silicon nitride, and parylene.

Silicon Dioxide

Devices with up to 1 μm oxide layers could be successfully fabricated. Upon testing, they showed some amount of shielding, but there was still significant capacitance variation with humidity. Thicker layers could not be used due to adhesion problems. Once thicker layers were deposited and patterned, it was noticed that parts of layer would break off.

Silicon Nitride

Thick layers of nitride could be successfully deposited and patterned without any adhesion or break-off problems. However, this material did not show any indication of shielding moisture. The sensitivity was almost the same as a device without the nitride layer. It was concluded that the silicon nitride is very porous and the moisture diffuses right through it.

Parylene

This material showed the best resistance to moisture. Fig. 10-3 shows the capacitance against relative humidity plot for a device with and without parylene protection. As can be seen, the sensitivity is reduced quite a bit by the parylene, especially for relative humidity levels below 70 %. However, for higher humidity levels, there is a fair amount of sensitivity. The thickness of parylene used was 900 nm and it is possible that thicker layers will shield much better. Unfortunately, thicker layers could not be used due to adhesion problems. Once thicker layers were deposited and patterned, they would start

peeling off. In the next phase of this project, chemical vapor deposition (CVD) recipes will be developed and optimized for depositing thicker layers using adhesion promoters.

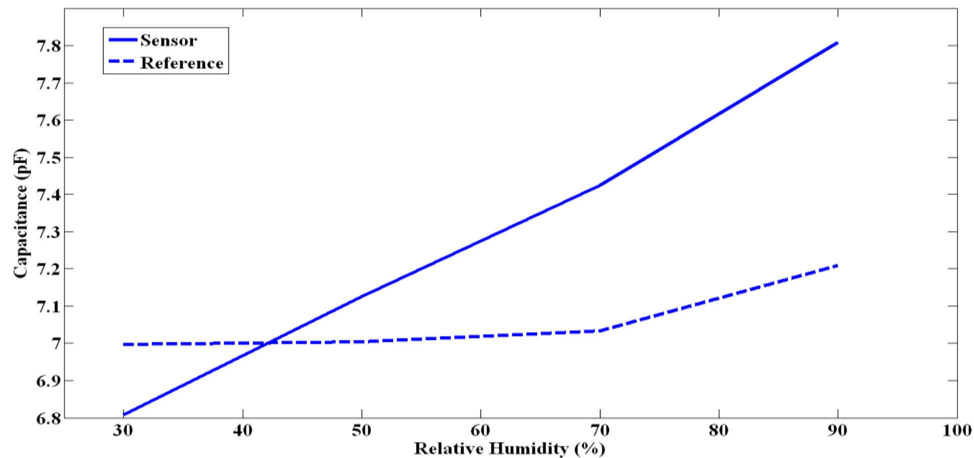

Figure 10-3: Plot of capacitance against relative humidity for a device with and without 900 nm parylene shield

3.3. CMOS Integration

3.3.1. Background on MEMS/CMOS Integration

MEMS components or systems have to be interfaced with their control and signal processing CMOS circuitry. This is referred to as CMOS integration of MEMS. There are two main methods to achieve this integration. The first is *hybrid* integration in which the MEMS and IC are on separate dies placed in the same package and interconnected using bond wires. The second integration method is referred to as *monolithic* integration in which the MEMS and IC are on the same die.

Majority of MEMS products today are hybrid integrated with their associated IC. Hybrid integration allows for a shorter development cycle as well as the independent optimization of the MEMS and IC components. However, the assembly and packaging costs are higher. Monolithic integration allows for a smaller, compact system in which only one die is placed in the package. Having only one die reduces the packaging complexity, which is a huge part of production costs. It also increases the reliability since

the number of off-chip connections is reduced. The MEMS and IC are interconnected on-chip and the use of bond wires for interconnecting both is eliminated. This reduces performance-limiting parasitic effects for both the MEMS devices and the IC. This is particularly important when there are many interconnections between the MEMS and CMOS. On the other hand, since the MEMS and IC are processed on the same die, longer development times and a higher initial investment are required. These disadvantages can be negated if high volume batch-manufacturing is done. In that case, the lower assembly and packaging cost makes up for the longer development time and higher initial investment.

Monolithic integration favors miniaturization, compactness, reliability, and increase in overall system performance. The industry is constantly driving towards the monolithic integration of MEMS and CMOS, in order to achieve fully-monolithic systems with the MEMS devices and the associated electronics on the same die. There are three ways to monolithically integrate MEMS with CMOS:

1) MEMS First or Pre-Processing -
   This involves fabricating the MEMS first, followed by the CMOS.
2) Interleaved Processing -
   CMOS and MEMS are fabricated in a single process flow. Basically, the fabrication steps for the MEMS process and CMOS process are carried out in parallel, but in an interleaved fashion.
3) MEMS Last or Post-Processing -
   In this case, the CMOS is fabricated first, followed by the MEMS. The MEMS is usually fabricated on top of the IC die.

The first two methods are usually used for MEMS processes that require a high thermal budget. For the interleaved processing [3], the standard CMOS process flow will be altered and this can cause reliability issues for the IC as well as an increase in the development time. Since both MEMS and CMOS processes run in parallel, this technique

of integrating MEMS and CMOS is very expensive. Very often, existing materials from the IC process are used to define layers of the MEMS devices and since these materials are usually chosen to favor electronic performance, there may a tradeoff between optimal MEMS or IC performance.

With pre-processing [4, 5], both processes are independent of each other and hence, there are no changes introduced in the standard CMOS process flow. However, the process is complicated since the MEMS have to be fabricated in a way that minimizes topographical errors for the subsequent CMOS process. Also, interconnecting the MEMS and CMOS is difficult since the MEMS have to be protected during the CMOS process flow. These disadvantages impose a lot of restrictions on the MEMS process flow steps and hence, the varieties of applications that can be monolithically integrated by MEMS pre-processing are highly limited.

With post-processing [6, 7], the integration is carried out after the IC process flow has been completed. The MEMS process flow has to be compatible with the IC in terms of the temperature and chemicals used. However, there is great versatility in terms of the thicknesses and materials that can be used to define the layers of the MEMS devices. As a result, materials like silicon carbide, which possesses very desirable mechanical properties, can be used as a MEMS layer without any effects on the IC performance. With post-processing, there is no alteration to standard CMOS processes. State-of-the-art CMOS foundries can be used to fabricate the IC and the MEMS can then be grown on top of the IC die. The IC and MEMS process can be combined into a single process flow or two separate process flows. In the latter case, the IC can be fabricated in one facility and the MEMS process flow can be carried out in another facility. This provides a very desirable flexibility.

For MEMS processing in university clean rooms, post-processing is perhaps the only option because academic fabrication facilities usually don't have the capabilities for carrying out interleaved or pre-processing techniques. MEMS last approach is beneficial since individual CMOS dies can be obtained from a second party and the MEMS can then

be fabricated on top of the IC die. This is the process that was used in this work do demonstrate a practical and convenient prototype method for integrating MEMS and IC. Commercial transimpedance amplifier (TIA) dies were obtained from Texas Instruments and the humidity sensors were then grown on top of these dies. The integration process used to successfully grow working sensor devices on top of the TIA dies is described next.

3.3.2. CMOS Integration Process Description

As mentioned earlier, the MEMS-last or post-processing approach was used in this work to integrate the humidity sensors with CMOS [10]. Since dedicated microfabrication masks were not made for CMOS integration, it was much desirable to work with individual IC dies instead of using whole semiconductor wafers. This also reduces cost and wastage since this work is only at the MEMS process development and prototyping stage. In this work, the intention was to report and use a prototype method to demonstrate the capability to successfully integrate the MEMS sensors with IC. Therefore, individual CMOS dies were used for this purpose. The sensor devices were fabricated on top of transimpedance amplifier (TIA) dies obtained from Texas Instruments. Normally, the sensors will be integrated with their associated control and signal processing IC, but the goal was to demonstrate the capability of integrating the MEMS sensors with any CMOS IC. Hence, TIA dies from Texas Instruments were used for this purpose. Figure 11-3 shows the TIA die used.

Figure 11-3: TIA die obtained from Texas Instruments

Fabricating MEMS on top of a single IC die is quite difficult since the handling of the IC becomes a major issue. The dies have to survive steps such as wet etching, spin-coating, and spin washing and drying. It is quite easy to damage or lose the dies during such

treatments. Also, equipment in university clean rooms usually process whole wafers and not individual dies. Therefore, in order to grow the humidity sensors on top of the CMOS die, the die had to be attached to a carrier wafer and then processed. The attachment has to be done so that the die holds firmly to the wafer for the entire process flow and survives all steps without falling off or getting damaged. It was found that a thin layer of a certain type of finely cured polymer can be used to stick the TIA die to the carrier wafer and this holds adequately for the entire MEMS humidity sensor process flow.

However, simply sticking the CMOS die to the carrier wafer is not sufficient. The problem of edge beads need to be avoided. Since the attached die introduces a significant step in the wafer surface, any sort of spin-coating will introduce massive edge beads (Fig. 12-3). The MEMS process flow involves a lot of patterning using photolithography. This implies that the CMOS die and the carrier wafer have to be spin-coated with photoresist at several points during the process flow. The edge-beading effect will cause the resist at the edges of the die to be thicker than the center of the die. During photolithography, these edge beads can significantly degrade the quality of the patterning around the edges of the die or completely prevent it. Hence, it is very crucial that these edge beads be avoided. A very good method of achieving this is to create a mold for the die. The die will be placed in the center of the mold with its active surface facing up. The mold serves to extend the effective planar surface of the die and any edge beads after coating resist will occur at the edges of the mold and not the die.

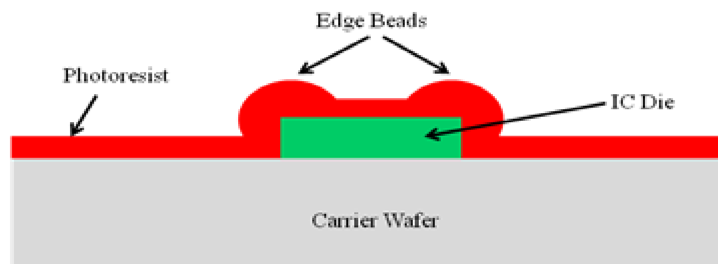

Figure 12-3: Cross-section of die on carrier wafer showing edge-beading effect from spin-coating photoresist

In [8], custom molds are used to hold the dies. However, with very small dies, placing and picking up the dies from these cavities has to be done with great accuracy and care. Also, a custom mold has to be made for every different sized IC die. In this work, a very

reliable method was reported for creating a mold for the CMOS die, regardless of its size [10]. The die is embedded in the mold during the mold creation process and is very easy to remove later. This mold, with the die in the center, is then attached to a carrier wafer, which is then processed to grow the humidity sensors on top of the IC die. The process steps of creating the mold and attaching it to a carrier wafer are described below.

a) Making a layer of Polydimethylsiloxane (PDMS)

XGE RTV615 (silicone rubber compound in liquid form) and its curing agent are mixed in a ratio of 3:1 respectively. The mixture is then stirred for about 5 minutes and poured in a Petri-dish to about 25% of the dish's height. It is then allowed to settle and distribute evenly, after which it is placed in a desiccator for about 10 minutes to remove all bubbles. There may still be bubbles left after removing from the dessicator. Holding the dish about 10 inches above a smooth surface and dropping it bottom flat on the surface several times serves to remove all remaining bubbles. The mixture is then cured in an oven at 60 °C for about an hour to induce polymerization and cross-linking of the material. This solidifies the mixture and forms a solid layer of PDMS.

b) Forming the mold to hold the die

The steps used to make the die mold and attach this mold to the carrier wafer are described next. The figure below shows the process flow steps and the description of each step follows after.

(1) Place the CMOS die face down on PDMS piece

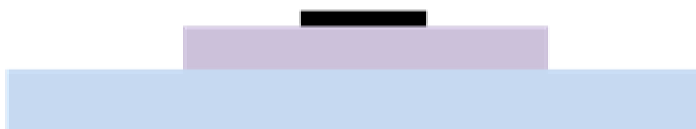

(2) Drop optical adhesive glue on top

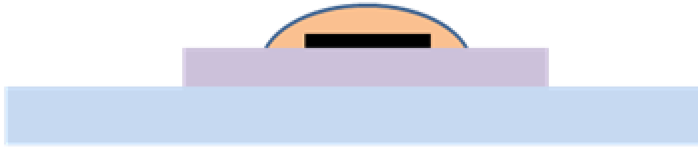

(3) Place a 2nd piece of PDMS on top

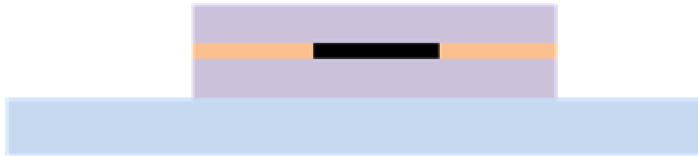

(4) Expose to UV light

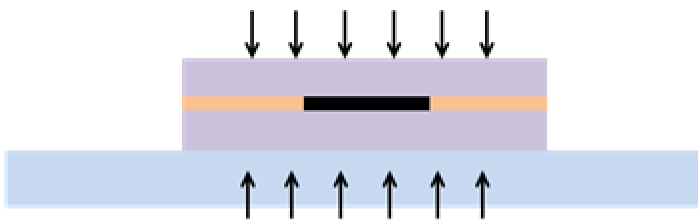

(5) Peel off the PDMS and glue layer

(6) Spin-coat the polymer / attach mold to carrier wafer

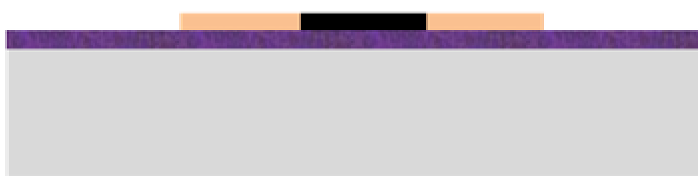

Figure 13-3: Steps for die mold fabrication and carrier attachment

(1) A blade is used to cut out two identical square pieces of the PDMS. Each side of the PDMS pieces should be around 5-6 times the length of the die. One PDMS piece is placed on a glass slide to facilitate handling and provide a flat working surface. The CMOS die is placed face down on the PDMS piece. A tweezer is used to slightly press down on the die and hold for a few seconds so that the die adheres to the PDMS surface and cannot move or slide around easily.

(2) Pour a drop or two of optically-curable adhesive glue (in liquid form) on the back of the die. Before placing the drops on the die, ensure that the glue drops are bubble free. This can be done by pouring several dummy drops elsewhere before pouring it on the die. The temporary adhesion between the die and the PDMS surface prevents the glue from seeping underneath and contaminating the active surface of the die. However, in some cases, a little bit of the glue may infiltrate and this can be removed in later steps.

(3) As soon as the optical glue is dropped on top of the die, place the other piece of PDMS gently on and press down VERY SLIGHTLY on all edges to level the glue layer at the same thickness as the die. It is very crucial that the pressing is done with very little force. Pressing a bit hard will form an uneven and inadequate mold for the die.

(4) After pressing very slightly on top of the second PDMS piece, expose immediately with UV light from both top and bottom for about 60 seconds each side. This cures and solidifies the glue.

(5) Remove the top PDMS layer and gently remove the glue layer using a tweezer. The CMOS die will be contained within the glue layer, with its active surface exposed. The glue would have formed a well-leveled mold enclosing the die. An illustration of this mold is shown in Fig. 14-3.

Figure 14-3: CMOS die mold with the CMOS die inside the mold

(6) Spin-coat the attaching polymer on the carrier wafer. Immediately place the die mold, with the exposed die active surface facing up, on top of the wafer and gently press down

on all sides of the mold. Then place the wafer in an oven at 200 ˚C for about 2 hours to cure the polymer. The curing solidifies the polymer and the die mold securely adheres to the carrier wafer surface.

c) Clean the die

Any residues that may be on the active die surface needs to be removed. Place the wafer in an Asher and expose to oxygen plasma for about 15 minutes. This etches away any glue that may be present on the die surface.

The CMOS die is now ready for MEMS processing. The humidity sensor fabrication process steps are carried out above-IC in the same manner as for a standard wafer substrate. After MEMS fabrication completion, the mold can easily be removed by applying a light mechanical force to all sides. The die can then be removed from its mold by using a razor blade. The removal process is very clean and repeatable.

All MEMS process steps were carried out in the same manner as in the fabrication of stand-alone sensors. The only difference was that the alignment for every photolithography step had to be done visually. To avoid this in the future, special masks will be made for CMOS integration which will have alignment marks for fabricating the MEMS on top of an IC die.

3.3.3. CMOS Integration Test Results

One specific relative humidity sensor design was grown on top of the TIA CMOS die. This was a Design-B type device (top electrode patterned with square holes) with $W = W_{gap} = 10$ µm. The picture of the CMOS die with the MEMS sensor on top is shown in Fig. 15-3. The size of the CMOS die is around 654 µm x 1030 µm. The area of the sensor grown on top is around 210 µm x 210 µm (without the GSG pads). A dedicated package and PCB was designed to hold the MEMS-processed TIA CMOS die.

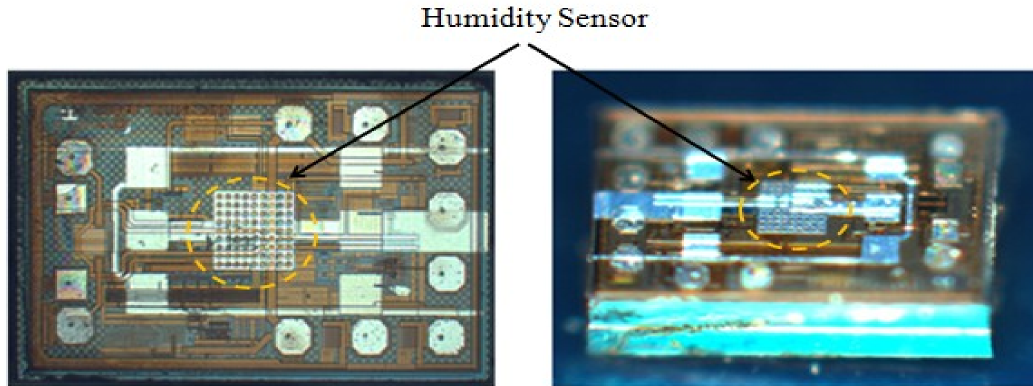

Figure 15-3: TIA CMOS die with MEMS sensor on top

TIA S-Parameters

The first tests done were to verify that the MEMS processing did not alter the performance of the CMOS TIA. This was done by comparing the S-parameters of the TIA before and after growing the humidity sensor on top of it. The S-parameter plots are shown in Fig.16-3 below. The solid lines represent the curves obtained before MEMS processing, while the dashed lines represent the curves obtained after the sensor had been grown on top. As can be seen, the correlation between both is quite close. Some oscillations can be noticed, but these are due to capacitive loading of the test setup and not due to the IC itself.

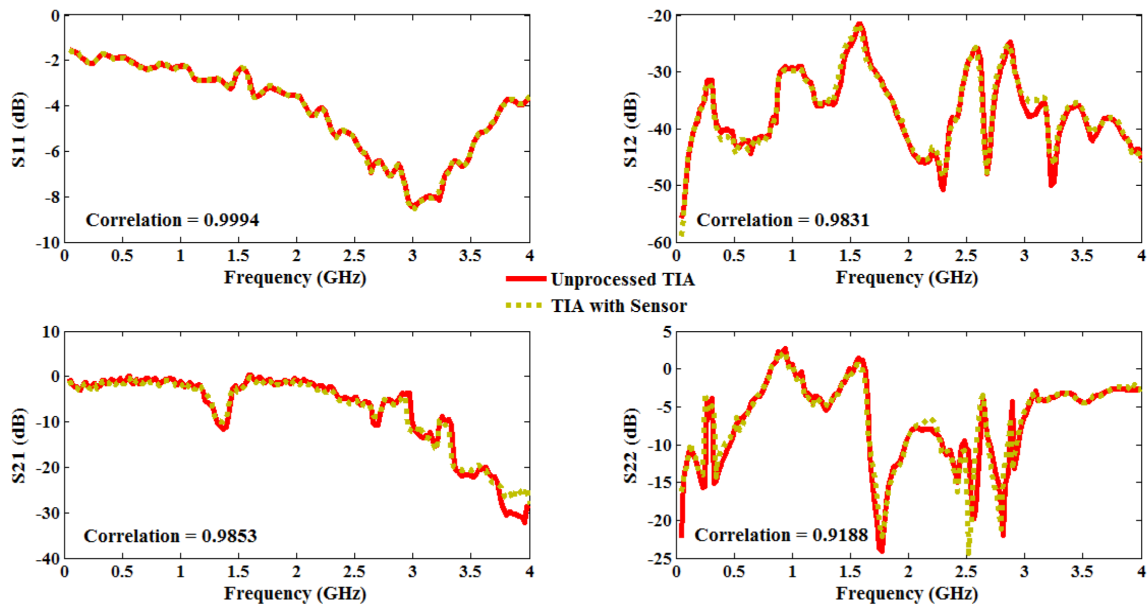

Figure 16-3: S-parameter plot for bare TIA die and TIA die with sensor grown on top

** Plots courtesy of Mr. Karim Allidina

Sensor Sensitivity and Hysteresis

Next, the MEMS sensor on top of the CMOS die was tested to verify that it was functional. A humidity chamber was used to cycle the relative humidity between 30 to 90 %RH at 25 ^{0}C. At this temperature, the minimum humidity the chamber can maintain is 30 %RH. To test the sensor at lower humidity levels, the temperature was increased to 50 ^{0}C and the humidity was cycled between 10 to 90 %RH. The plots of sensor capacitance against humidity at both temperatures are shown in Fig. 17-3. The performance parameters are shown in Table 4-3.

The sensitivity of the CMOS integrated sensor is lower than the corresponding stand alone sensor (21.7% vs. 22.5%). This can be due to higher parasitic capacitances from the CMOS die or simply due to process variations and measurement inaccuracies. The sensitivity increases at a higher temperature as expected. It can be noticed from the results that the hysteresis also increases with temperature.

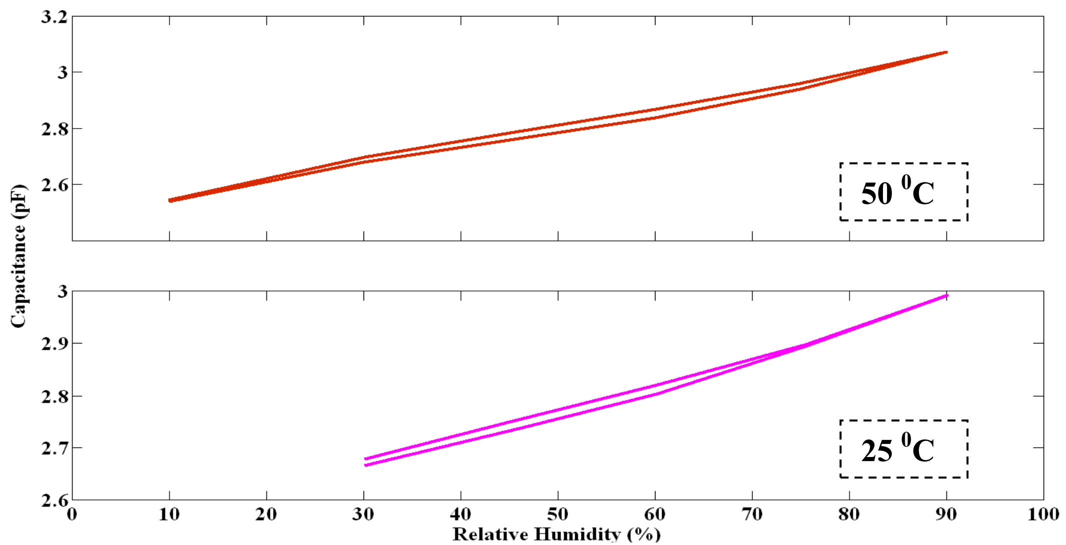

Figure 17-3: Sensor capacitance vs. relative humidity for the MEMS sensor grown on top of CMOS die

	25 ^{0}C	50 ^{0}C
Sensitivity	21.7 %	25.9 %
Max Hysteresis	3.4 %RH at 60 %RH	4.19 %RH at 60 %RH
Linearity (R^2)	0.9911	0.9927

Table 4-3: Performance parameters for the MEMS sensor on top of CMOS die

Sensor Repeatability

The sensor capacitance variation as humidity is varied from 30 to 90 %RH was measured three different times to test how repeatable the results are. The plots for each of the 3 runs are shown in Fig. 18-3. As can be seen, the results are very repeatable. The maximum difference between the curves is around 0.5 % at 90 %RH. As mentioned earlier, the chamber humidity constantly fluctuates, and this fluctuation is larger at high humidity levels – up to 8% variation at 90%RH. This chamber humidity fluctuation could be a contributing factor to the slight difference in sensor capacitance in each of the 3 runs.

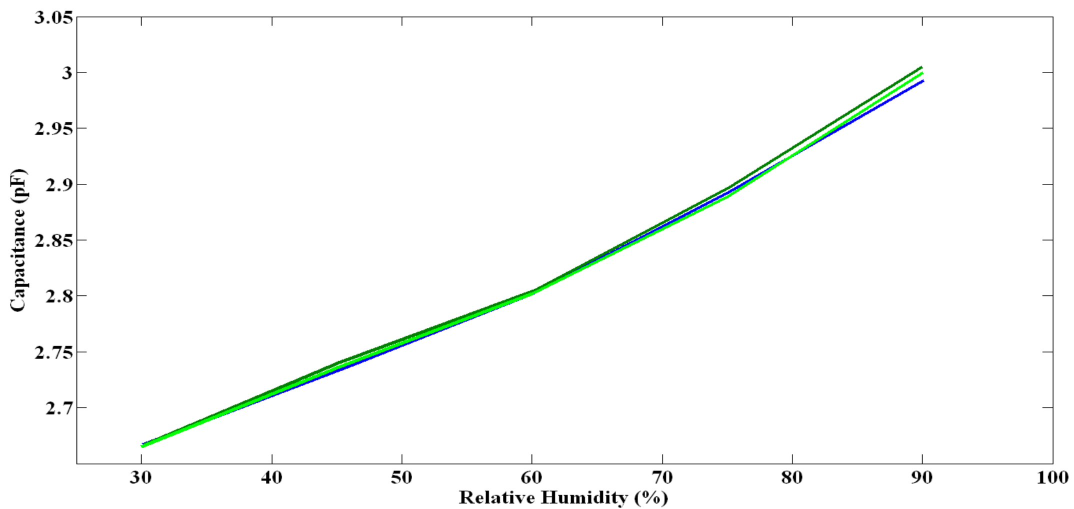

Figure 18-3: Sensor capacitance vs. relative humidity for 3 different test runs

Sensor Response Time

The response of the sensor to a humidity step from room humidity (~40 %RH) to 70 %RH is shown in Fig. 19-3 along with the response of a stand-alone sensor and the simulated response for the same design. As can be seen, the response of the CMOS-integrated sensor is faster than the stand-alone sensor (**25 s** and 30.8 s respectively). The difference could be due to thinner or narrower regions of the polymer (resulting in lower diffusion time) as a result of the highly non-planar nature of the CMOS die surface and due to process variations.

The response time of the integrated sensor is high due to the large top metal width (W = 10 μm). Faster devices were not integrated due to size limitations. Only a few devices on the mask were small enough to fit within the CMOS die dimensions without shorting out or insulating the CMOS connection pads and they were the slower devices. In the next phase of the project, dedicated masks will be made for CMOS integration to avoid such issues.

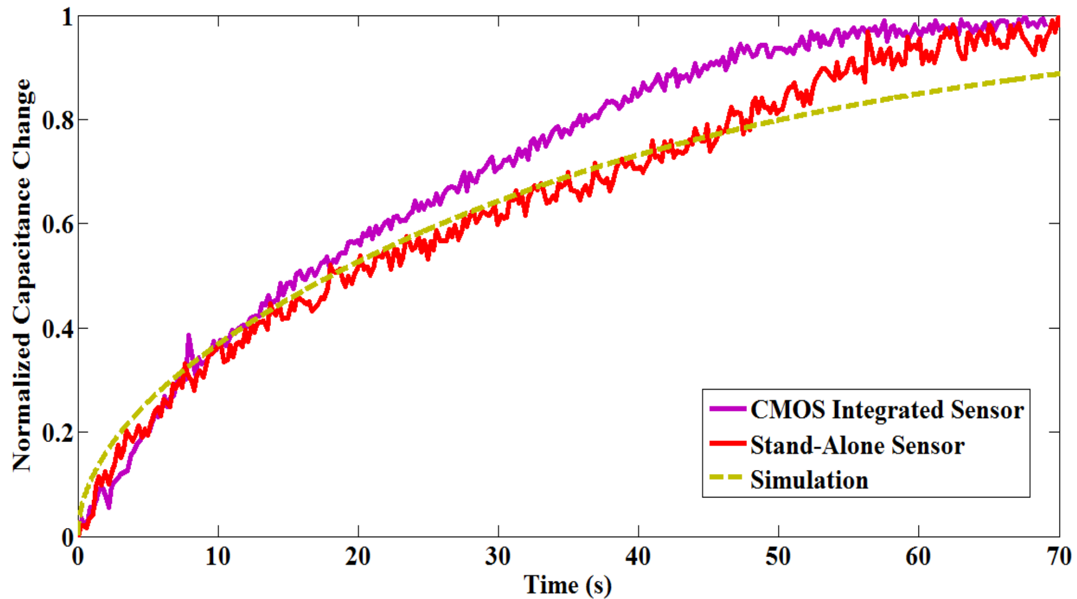

Figure 19-3: Relative humidity step (40 %RH to 70 %RH) response of sensor device grown on top of CMOS die along with the response of the stand-alone sensor and the simulation response

3.4. References

[1] Vaisala Humidity Calibrator HMK15 User's Guide (http://www.vaisala.com/)

[2] R. DeIasi and J. Russell, "Aqueous degradation of polyimides", *Journal of Applied Polymer Science*, Vol. 15, pp. 2965-2974, 1971.

[3] G. Abadal, et al., "Monolithic integration of MEMS resonators in a 0.35 μm CMOS technology for gravimetric sensor and radiofrequency applications", *Integration Issues on Miniaturized Systems – MOMS, MOEMS, ICS and Electronic Components (SSI)*, pp. 1-8, 2008.

[4] Y. B. Gianchandani, et al., “A MEMS-first fabrication process for integrating CMOS circuits with polysilicon microstructures”, *Micro Electro Mechanical Systems*, pp. 257-262, 1998.

[5] J. H. Smith, et. Al., “Embedded micromechanical devices for the monolithic integration of MEMS with CMOS”, *Electronic Devices Meeting*, pp. 609-612, 1995.

[6] J. P. Busquere, et. Al., “Above IC MEMS capacitors for integrated reconfigurable circuits”, *Microwave Conference Proceedings*, pp. 4, 2005.

[7] D. Saias, et al., “An above IC MEMS RF switch”, *Journal of Solid-Sate Circuits*, vol. 38, pp. 2318-2324, 2003.

[8] A. G. Mukherjee, M. E. Kiziroglou, A. S. Holmes, and E. M. Yeatman, “Die-Level Integration of Metal MEMS with CMOS”, *2nd Electronics System-Integration Technology Conference*, pp. 160-173, Sep. 2008.

[9] N. A. Dotson, P. T. Kim, and A. Mason, “Low Cost MEMS Processing Techniques”, *ASEE/NCS*, April 2004.

[10] P. V. Cicek, Q. Zhang, T. Saha, S. Mahdavi, K. Allidina, F. Nabki, and M. N. El-Gamal, “*A Novel Prototyping Method for Die-Level Monolithic Integration of MEMS Above-IC*”, Journal of Micromechanics and Microengineering (IOP Science), 2012 – not published yet, under review.

4. Conclusion

Using all the simulation and measurement results obtained, a design strategy was developed for MEMS capacitive relative humidity sensors. This is discussed below.

4.1. Design Strategy

(a) **Use minimum top and bottom electrode thickness –** maximizes sensitivity
(b) Minimize polymer thickness – improves sensitivity and response time
(c) Keep bottom electrode flat – reduces hysteresis
(d) Pattern the top electrode as rectangular fingers – best response/recovery time and also provides better long term drift
(e) **Use minimum top electrode width –** fastest response/recovery time
(f) **Keep the gap between fingers the same as finger width –** larger gaps will reduce sensitivity and smaller gaps will worsen long term drift
(g) **Minimize sensing area and electrode overlap area –** improves long tern drift

(a) Using minimum thickness for top and bottom electrodes maximizes sensitivity. The sputtering recipes developed for depositing the electrodes allowed thicknesses as low as 60 nm.

(b) Sensitivity and response time are both improved with a thinner polymer layer. Recipes were developed for depositing sensing polymer layers as thin as 100 nm.

(c) Patterning the bottom electrode to be identical to the top electrode improves sensitivity, but the hysteresis increases. The latter is much more pronounced than the former, and hence, it is preferable to avoid patterning the bottom electrode and keep it flat instead.

(d) Sensor devices with the finger structure show the fastest response and recovery times. Devices with holes patterned into the top electrode are slower. However, if holes are used, the shape of the hole is important. Square holes show the best response.

Long term drift is dependent on the area of the polymer that is part of the active capacitance of the device (i.e. the polymer between the overlap area between the top and bottom electrodes). Therefore, minimizing the electrode overlap area serves to reduce long term drift. The finger structure generally provides smaller overlap area since the overall top metal area is smaller, and hence shows less long term drift.

(e) The width of the top metal is very critical for the speed of the sensor. Minimizing this width maximizes the speed. However, the sensitivity is reduced slightly. The effect on the response time is significantly greater than the effect on sensitivity and this parameter should be optimized for response time.

(f) The width of the top metal opening should not be too large. This will reduce the sensitivity slightly. If it is too small, the electrode overlap area is increased and this will worsen the long term drift slightly. The effect of this parameter is not too significant. Using a gap size the same as the top metal width is sufficient.

(g) As mentioned already, long term drift is dependent on the area of the polymer that is part of the active capacitance of the device (i.e. the polymer between the overlap area between the top and bottom electrodes). Therefore, minimizing the sensor size serves to reduce long term drift. Using the mask and process flow developed in this work, a whole variety of sensor sizes can be fabricated. The table below shows the variety.

Sensing Area	Sensor Capacitance (pF)
1 mm x 1 mm	100
0.5 mm x 0.5 mm	25
0.25 mm x 0.25 mm	7
190 µm x 190 µm	4
170 µm x 170 µm	3
120 µm x 120 µm	1.5
80 µm x 80 µm	0.5

Table 1-4: Various sensor sizes that can be fabricated

4.2. Future Work

(1) The microfabrication masks used in this work were not designed for CMOS integration. As a result, only a few devices could be fabricated on top of the IC die and alignment during photolithography had to be done visually due to absence of CMOS die alignment marks. In the next phase of this work, dedicated masks will be made for CMOS integration which will have alignment marks for aligning MEMS with IC and allow a whole variety of devices to be grown on top of the IC die.

(2) Silicon Oxide and Nitride showed poor resistance to humidity, but parylene showed good resistance to moisture diffusion for use as the humidity shield in the reference devices. However, there was still some sensitivity. Thicker parylene layers could potentially provide the perfect shield, but could not be used due to adhesion problems. Future work will include developing recipes for depositing thicker parylene layers successfully and also researching on other possible materials that can be used as moisture shield.

(3) The heaters underneath the sensors were fabricated, but were not tested in this work. This will be done in the next phase of the project.

(4) Finally, many identical versions of the each design variation will be fabricated and the mean sensitivities will be compared in order to notice small differences in sensitivity between designs, which is otherwise not detectable due to process variations, parasitic capacitances, and measurement inaccuracies/errors.

4.3. Summary

A complete literature review on humidity sensors has been presented. Polymer-based MEMS capacitive relative humidity sensors were designed, fabricated, and tested. A completely CMOS compatible process flow was developed for the fabrication of the sensors. All the fabrication issues that were faced and their solutions have been outlined and discussed. Upon successful completion of fabricating the devices, various testing methodologies were devised and setup, which allowed the successful testing of all devices and specifications. Different designs were compared and analyzed based on simulation and experimental results, and these results were used to outline a design strategy for polymer-based MEMS capacitive relative humidity sensors.

Finally, the sensors were integrated with commercial CMOS dies. A simple and versatile process was reported and used for fabricating the sensors on top of IC dies of any size. Pre-integration and post-integration testing verified the MEMS process to be fully IC-compatible. Test results show the proper operation of both MEMS and electronics before and after integration.